Trade Study of a Thermally Insulated, Nonuniform, Single-Zone Absorption Cell

A Thesis Presented for the

Master of Science

Degree

The University of Tennessee, Knoxville

Waritphon Overacker

December 2019

© by Waritphon Overacker, 2019
All Rights Reserved.

I'd like to dedicate this thesis to my mother and father for their endless love, support, and sacrifice.

Acknowledgments

First and foremost, I would first like to thank my advisor, Dr. Trevor Moeller, for introducing me into his research group and guiding me through this project. I would also like to thank Dr. Monty Smith and Dr. Feng-Yuan Zhang for taking their time to serve on my committee. Thank you to Mr. Travis Johnson and Ms. Katrina Sweetland, former students who have worked on this project, for teaching me the experimental methods and for answering any questions that I had. A big thank you to Mr. Jonathan Kolwyck and Mr. Doug Warnberg for helping me set up and run my experiments; I would have been so lost without your assistance. Lastly, I would like to thank Mr. Andrew Fahrland, one of the designers of the laser absorption instrument, for taking the time to answer any questions I had. Thank you to everyone who has assisted, guided, and encouraged me along the way to the completion of this project. None of this would be possible without your help.

Abstract

Different chemical species have unique line spectra that contain information pertaining to their physical properties such as temperature, pressure, and species concentration. Line spectra must be calibrated with a high-temperature absorption cell in order to validate experimentally measured spectra with simulated spectra. The University of Tennessee Space Institute uses a high-temperature, single-zone absorption cell for spectral calibrations. Tunable diode laser absorption spectroscopy (TDLAS) is the diagnostic technique used in this research to measure temperature and species concentrations of CO and CO_2 mixtures in the absorption cell. However, TDLAS takes the path-average measurement of the line-of-sight, which is problematic because the absorption cell suffers from a nonuniform temperature distribution across the heated path. Thermal insulation is applied to the absorption cell in order to reduce that temperature gradient. The research presented in this thesis studies the effects that a reduced temperature gradient has on accuracy of the measured temperature and species concentration for a 3% CO/97% N_2 and 1% CO_2/99% N_2 mixture. Results show that insulation was effective at improving the overall temperature measurement accuracy of CO by reducing the percentage difference of measured to known values from 21% - 59% to 0.70% 8.6%; however, CO_2 temperature measurement accuracy only improved half of the time. Unfortunately, the measurement system was unable to produce meaningful results for CO species concentrations, but CO_2 species concentrations produced reasonable results that demonstrated an increase in percentage difference of measured to known values from 55% - 155% to 87% - 161% once the insulation was applied. These results indicate that insulation showed improvement in measurement accuracy for some cases, and that the data contained inconsistencies and non physical results. Therefore, a better correction system for the nonuniform temperature distribution is required.

Table of Contents

1 Introduction **1**

1.1 Motivation 1

1.2 Uncertainty Issue 2

1.3 Objective 3

1.4 Organization 3

2 Background **4**

2.1 Electromagnetic Radiation 4

2.2 Absorption Spectroscopy 5

3 Setup and Experimentation **9**

3.1 Line Selection and Spectral Databases 9

3.2 UTSI Spectroscopy Lab 10

3.2.1 Laser Measurement and Detector Setup 11

3.2.2 High Temperature Absorption Cell Setup 12

3.3 Proposed Three-Zone Absorption Cell Design 16

3.4 Thermal Insulation 17

3.5 Temperature Distribution Tests 18

3.6 Absorption Cell Testing 22

4 Results and Discussion **25**

4.1 Data Collection & Post Processing 25

4.2 CO Results 31

4.3 CO_2 Results 42

5 Conclusions and Recommendations **53**

5.1 Conclusions 53

5.2 Recommendations for Future Work 55

Bibliography **57**

Appendices **61**

A Temperature Distribution Test Results and WinOSC Layers **62**

B Gas Premixing Procedure **75**

C Raw Data Plots **77**

Vita **79**

List of Tables

4.1 Goodness of Fit for Measured CO data (insulated) 40

4.2 Goodness of Fit for Measured CO data (uninsulated) 40

4.3 Measured results vs. known vaules of temperature and species concentration with insulation. 41

4.4 Measured results vs. known vaules of temperature and species concentration without insulation. 42

4.5 Goodness of Fit for Measured CO_2 data (with insulation) 52

4.6 Goodness of Fit for Measured data (without insulation) 52

4.7 Measured results vs. known vaules of temperature and species concentration for CO_2 (with insulation). 52

4.8 Measured results vs. known vaules of temperature and species concentration (without insulation). 52

A.1 Table of a half profile temperature distribution comparing insulated and uninsulated ends for a furnace setting of $250°C$. (*centerline of absorption cell/furnace) 63

A.2 Layer inputs used to simulate a nonuniform temperature distribution with uninsulated quartz ends for a furnace setting of 250°C [523 K] 64

A.3 Layer inputs used to simulate a nonuniform temperature distribution with insulated quartz ends for a furnace setting of 250°C [523 K]. 64

A.4 Table of a half profile temperature distribution comparing insulated and uninsulated ends for a furnace setting of $500°C$. (*centerline of absorption cell/furnace) 66

A.5 Layer inputs used to simulate a nonuniform temperature distribution with uninsulated quartz ends for a furnace setting of 500°C [773 K]. 67
A.6 Layer inputs used to simulate a nonuniform temperature distribution with insulated quartz ends for a furnace setting of 500°C [773 K]. 67
A.7 Table of a half profile temperature distribution comparing insulated and uninsulated ends for a furnace setting of 750°C. (*centerline of absorption cell/furnace) 69
A.8 Layer inputs used to simulate a nonuniform temperature distribution with uninsulated quartz ends for a furnace setting of 750°C [1023 K]. 70
A.9 Layer inputs used to simulate a nonuniform temperature distribution with insulated quartz ends for a furnace setting of 750°C [1023 K]. 70
A.10 Table of a half profile temperature distribution comparing insulated and uninsulated ends for a furnace setting of 900°C. (*centerline of absorption cell/furnace) 72
A.11 Layers used for a furnace setting of 1173 K with uninsulated quartz ends. . . 73
A.12 Layers used for a furnace setting of 1173 K with insulated quartz ends. . . . 73

List of Figures

2.1 Three processes of emission or absorption where E is the energy of a photon between lower energy state, m, or a higher energy state, n [1]. 6

3.1 Schematic of UTSI's TDLAS setup drawn by Katrina Sweetland [2]. The optical breadboard on the left mounts the laser system while the one on the right mounts the detectors. The test gas section in the center is where the absorption cell is located. 13

3.2 WinOSC simulated spectra for 3% CO, 1% CO_2, and 1.9% H_2O for the 5.16 μm and 2.74 μm laser. 14

3.3 UTSI's Carbolite ® tube furnace with a quartz tube placed through the center and supported by steel flanges. 15

3.4 Drawing of the proposed three-zone cell design by Travis Johnson. [3]. 17

3.5 MaxWool^{TM} HPS ceramic fiber blanket used to insulate the quartz ends of the tube furnace. 18

3.6 High temperature absorption cell with the quartz ends insulated with the MaxWool^{TM} HPS ceramic fiber blanket. 19

3.7 A slide rail with an arm designed to mount a K-type thermocouple for axial temperature measurements through the tube furnace. 20

3.8 Full profile temperature distribution of the absorption cell at furnace setting of 900°C. 21

3.9 An air tank was used to premix the gases to desired concentrations using Dalton's Law of Partial Pressures. Valves and pressure transducers were used to control and monitor the gas pressure during premixing and absorption cell testing. 23

4.1 Laser sweep of 3% CO at room temperature as displayed on the Data Collection LabVIEW. Detector 1 (black line) represents the 5.16 μm laser and detector 2 (red line) represents the 2.74 μm laser. 26

4.2 Laser sweep of 3% CO with uninsulated ends at room temperature, 773K, and 1173K as displayed on the Data Collection LabVIEW. Detector 1 (black line) represents the 5.16 μm laser and detector 2 (red line) represents the 2.74 μm laser. 27

4.3 Corrected DC offset for 3% CO with uninsulated ends at room temperature, 773K, and 1173K as displayed on the Data Collection LabVIEW. Detector 1 (black line) represents the 5.16 μm laser and detector 2 (red line) represents the 2.74 μm laser. 28

4.4 Simulated spectra used to examine the behavior of CO and H_2O for different temperatures and species concentrations. 33

4.5 WinOSC simulated spectra for 3% CO and 1.9% H_2O at 523 K for a 5.16 μm laser. 34

4.6 WinOSC simulated spectra for 3% CO and 1.9% H_2O at 773 K for a 5.16 μm laser. 34

4.7 WinOSC simulated spectra for 3% CO and 1.9% H_2O at 1023 K for a 5.16 μm laser. 35

4.8 WinOSC simulated spectra for 3% CO and 1.9% H_2O at 1173 K for a 5.16 μm laser. 35

4.9 Measured vs. simulated spectra for 3% CO at 523 K with and without insulation for atmospheric pressure and a path length of 70 cm. 36

4.10 Measured vs. simulated spectra for 3% CO at 773 K with and without insulation for atmospheric pressure and a path length of 70 cm. 37

4.11 Measured vs. simulated spectra for 3% CO at 1023 K with and without insulation for atmospheric pressure and a path length of 70 cm. 38
4.12 Measured vs. simulated spectra for 3% CO at 1173 K with and without insulation for atmospheric pressure and a path length of 70 cm. 39
4.13 Simulated spectra used to examine the behavior of CO for different temperatures and species concentrations. 44
4.14 WinOSC simulated spectra for 1% CO_2 at 523 K for a 2.74 μm laser. 45
4.15 WinOSC simulated spectra for 1% CO_2 at 773 K for a 2.74 μm laser. 45
4.16 WinOSC simulated spectra for 1% CO_2 at 1023 K for a 2.74 μm laser. 46
4.17 WinOSC simulated spectra for 1% CO_2 at 1173 K for a 2.74 μm laser. 46
4.18 Measured vs. simulated spectra for 1% CO_2 at 523 K with and without insulation for atmospheric pressure and a path length of 70 cm. 47
4.19 Measured vs. simulated spectra for 1% CO_2 at 773 K with and without insulation for atmospheric pressure and a path length of 70 cm. 48
4.20 Measured vs. simulated spectra for 1% CO_2 at 1023 K with and without insulation for atmospheric pressure and a path length of 70 cm. 49
4.21 Measured vs. simulated spectra for 1% CO_2 at 1173 K with and without insulation for atmospheric pressure and a path length of 70 cm. 50

A.1 This plot represents how the layers for a temperature distribution of 523 K were divided for the WinOSC simulations. 65
A.2 This plot represents how the layers for a temperature distribution of 773 K were divided for the WinOSC simulations. 68
A.3 This plot represents how the layers for a temperature distribution of 773 K were divided for the WinOSC simulations. 71
A.4 This plot represents how the layers for a temperature distribution of 1173 K were divided for the WinOSC simulations. 74

B.1 Schematic of UTSI's gas premixing setup drawn by Katrina Sweetland. . . . 75

C.1 Corrected DC offset for 3% CO with insulated ends at room temperature, 773K, and 1173K as displayed on the Data Collection LabVIEW. Detector 1 (black line) represents the 5.16 μm laser and detector 2 (red line) represents the 2.74 μm laser. 77
C.2 MATLAB plot for voltage vs. sample number with corrected DC offset for 1% CO_2 for a test cell with uninsulated ends at room temperature (300K), 773K, and 1173K. 78
C.3 MATLAB plot for voltage vs. sample number with corrected DC offset of 1% CO_2 for a test cell with insulated ends at room temperature (300K), 773K, and 1173K. 78

Nomenclature

α	Spectral absorbance/optical depth (OD)
α_D	Doppler width
α_L	Lorentz width
$\bar{y}$	Mean value of the measured data set, n
χ_i	Mole fraction of absorbing species
$\hat{y}$	Predicted value of the measured data set, n
λ	Wavelength [m]
ν	Frequency [Hz]
ν_0	Transition line center wavenumber [cm^{-1}]
ν_c	Line-center frequency of the transition [Hz]
ϕ_ν	Line shape function
τ	Modified Thompson Tau constant, 2
$\widetilde{\nu}$	Wavenumber [cm^{-1}]
A_i	Area of natural log of transmittance for transition i
c	Speed of light in a vacuum, 2.9979925 x 10^8 [m/s]
E	Energy of a photon

E'' Lower state energy

E_m Ground state

E_n Higher energy level

h Planck's constant, 6.62607004 x 10^{-34} $\left[\frac{m^2 kg}{s}\right]$

I_0 Incident intensity

I_t Transmitted intensity

K Voigt function

k Boltzmann constant, 1.38064852 x 10^{-23} $\left[\frac{m^2 kg}{s^2 K}\right]$

L Laser path length [cm]

N Number density of the absorbing species

n Number of data points used to generate the spectra

n_A Avagadro's number, 6.02214 x 10^{23} [molecules/mo]l

P Static pressure of the gas [atm]

P_i Partial pressure of the absorbing species [psia]

P_T Total pressure of the gas mixture [psia]

$Q(T)$ Rovibrational partition function at gas temperature T for species of interest

$Q(T_0)$ Rovibrational partition function at HITRAN referenced temperature T_0

R Universal gas constant, 8.314472 $\left[\frac{J}{K \cdot mol}\right]$

$S(T)$ Line strength scaled to temperature T $\left[\frac{cm^{-1}}{molecule \cdot cm^{-2}}\right]$

$S_0(T_0)$ Reference linestrength $\left[\frac{cm^{-1}}{molecule \cdot cm^{-2}}\right]$

s_x Standard deviation of the data set, x

T	Gas temperature [K]
T_0	HITRAN referenced temperature, 296 K
T_ν	Transmittance
x	Data set of temperature or species concentration from the post processing software
x_i	Value of a measured point in the data set, x
y_i	Value of a measured point for data set, n

Chapter 1

Introduction

1.1 Motivation

Utilization of the combustion process has driven the growth of civilization through advances in industry, transportation, and power generation. As the world becomes more reliant on combustion, it has become necessary to develop tools that monitor combustion systems based on economic and environmental concerns. Incomplete combustion not only leads to power inefficiencies, but also emits harmful pollutants that are detrimental to the environment and human health. Monitoring of chemical species found in combustion byproducts will allow people to take corrective measures when designing combustion systems.

Developing technologies in the aerospace industry rely on improving the efficiency of the combustion process to create faster and more powerful air vehicles. Further research into supersonic combusting flows appears to be a promising field of study for these goals to be realized. In general, supersonic flows are identified as having flow speeds between Mach 1 and 5, and they exhibit unique properties that make study in this flight regime different than the subsonic regime of commercial aircraft. One such difference is that the effects of compressibility are much more prominent, and the fluid density can no longer be assumed constant. Shockwaves, discontinuities in the flow field, cause abrupt changes in the flow properties, such as velocity, pressure, temperature, and density [4]. Proper combustion must occur at the appropriate flow conditions; therefore, diagnostics are of great interest to research of these flows as they allow for monitoring of such parameters so that design changes

and optimization can be made to improve efficiency. Traditionally, probes are placed within the flowpath to collect engine data. However, flow conditions are harsher and more sensitive to disturbances in the supersonic regime. Such intrusive methods as exposing a probe in the flowpath requires active cooling and can have large uncertainty; they can also alter the flow properties. Therefore, researchers have looked to nonintrusive diagnostic methods such as tunable diode laser absorption spectroscopy (TDLAS) for monitoring of such parameters.

TDLAS was developed in the 1970s and is a popular method used in combustion diagnostics due to its nonintrusive nature and fast response time [2]. As opposed to its intrusive counterparts, nonintrusive methods are much more cost efficient and able to withstand harsh environments in the engine flowfield. TDLAS takes advantage of the unique absorption spectra that all chemical species generate to allow for the identification of flowfield parameters of interest such as temperature, velocity, pressure, and species concentration [5]. TDLAS measurements, however, rely on simulated spectra for selecting the correct laser, spectral ranges, and extracting the desired flowfield parameters. Simulated spectra gathers information for the species of interest from spectral databases and must be calibrated with a high-temperature absorption cell to verify measurements [2].

1.2 Uncertainty Issue

The University of Tennessee Space Institute (UTSI) is using a laser diagnostic system paired with a high temperature, single-zone absorption cell for laser absorption spectroscopy in the mid-infrared. The purpose of the system is to serve as an absorption line calibration device by measuring the temperature and concentration of sample gas mixtures for common combustion products such as CO, CO_2, and H_2O and comparing them to results from simulated spectra. The mid-infrared band is of interest due to the availability of absorption features for typical combustion products that contain the highest interaction strengths between commerically available lasers [6]. The current cell, however, suffers from a large temperature nonuniformity that affects the accuracy of the results. Laser absorption spectroscopy takes the path average value of the laser's line-of-sight. While nonuniform conditions are common when performing combustion diagnostics in practical applications,

correcting for the nonuniformities can become quite tedious when trying to take accurate measurements for calibration. UTSI proposed the development of a three-zone absorption cell inspired by a similar design from the University of Denmark [3, 7]. The proposed cell addresses the temperature uniformity issue while also adding the capability for real time temperature measurements. During the time of this thesis, funding for the development of the proposed three-zone abosrption cell was currently pending. While funding details are being resolved, a temporary solution for reducing the high temperature gradient is being applied so that a study can be performed on how a reduced temperature gradient affects the results of the measured spectra compared to simulated spectra.

1.3 Objective

The purpose of this thesis is to investigate the effects that the high temperature gradients have on the reduction of the temperature gradient, and study/compare the effects of how a decreased temperature gradient across the absorption cell would have on the accuracy of the results. A comparison between the normal temperature gradient and reduced temperature gradient is made by comparing their concentrations and temperatures obtained from a measured spectra to simulated spectra. A reduction in measurement uncertainty is greatly desired.

1.4 Organization

Chapter 2 provides background and theory related to the understanding of absorption spectroscopy. Chapter 3 details the laboratory setup and provides information on the materials, equipment, and software used during the experimentation process. Experimental procedures are discussed and some representative test results and simulations are also featured in this chapter. Chapter 4 discusses the results of the experimentation. Chapter 5 provides concluding remarks and discusses what the author believes should be done in order to move the project forward.

Chapter 2

Background

2.1 Electromagnetic Radiation

Electromagnetic radiation is a form of energy that can be described as a transverse wave where the two perpendicular fields oscillating in phase are an electric and magnetic vector. All forms of matter emit some type of electromagnetic radiation at varying frequencies, wavelengths, and energies that can be quantified on the electromagnetic spectrum. The electromagnetic spectrum is divided into 7 bands. Labeling them in increasing energy, these bands are as follows: radiowaves, microwaves, infrared, visible light, ultraviolet, x-rays, and gamma rays. Each band has a unique quantum mechanical property that describes the interaction between the chemical bonds within the species. These interactions between the electromagnetic spectrum and matter can be studied in a field known as spectroscopy.

For any region on the electromagnetic spectrum, the wave will oscillate at a constant speed in a vacuum [8]. This speed is known as the speed of light, c, and can be expressed as the product of the wavelength, λ, and its frequency, ν, as shown in equation (2.1).

$$c = \lambda\nu \tag{2.1}$$

Rearranging equation (2.1) yields a common unit used in spectroscopy known as the wavenumber. The wavenumber, $\widetilde{\nu}$, given by (2.2)

$$\widetilde{\nu} = \frac{\nu}{c} = \frac{1}{\lambda} \tag{2.2}$$

is the spatial frequency of a wave. It describes the number of waves per some unit length, which is commonly the centimeter. The wavenumber is also directly proportional to the energy of a photon, E, through the Bohr equation (2.3)

$$E = h\nu = hc\widetilde{\nu} \tag{2.3}$$

where h is Planck's constant and ν is the frequency. This relationship enables people to easily compare the energy values between spectral peaks with numbers that are easy to conceptualize. Each atom or molecule has innate energy levels at which they exist. When a species interacts with electromagnetic radiation, a photon can be either emitted or absorbed depending on the required energy level of the chemical species and whether the energy is emitted or absorbed.

There are three processes that may occur when electromagnetic radiation interacts with an atom or molecule as shown in Figure 2.1. The first process is induced absorption, occuring when an atom or molecule absorbs the required amount of radiation to become excited into a higher energy level, E_n. The second process is spontaneous emission. Atoms or molecules do not maintain their excited state for long and will eventually return to their ground state, E_m, by emitting radiation equivalent to the amount of energy that was absorbed to reach the excited state. The final process is stimulated emission where an atom or molecule emits a photon to reach a lower energy state. Unlike spontaneous emission, this process does not happen naturally but results when radiation of a specific wavenumber induces the atoms or molecules into a lower energy state [1]. Absorption spectroscopy is the diagnostic technique used in this research and relies on the process of induced absorption for its analysis.

2.2 Absorption Spectroscopy

Specific bands of electromagnetic radiation can be absorbed and used to determine more information about the medium through which the waves pass in a technique known

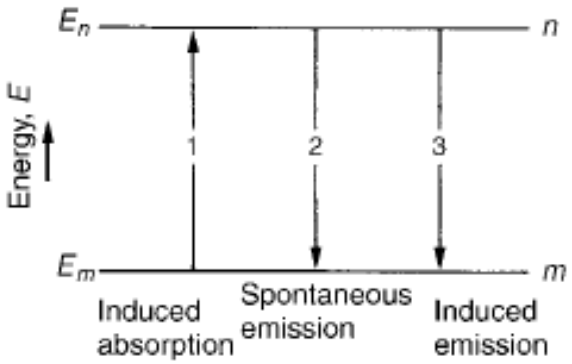

Figure 2.1: Three processes of emission or absorption where E is the energy of a photon between lower energy state, m, or a higher energy state, n [1].

as absorption spectroscopy. The Beer-Lambert Law is the foundation of absorption spectroscopy, and it describes the relationship between the incident and transmitted intensity of light traveling through a sample by relating its attenuation to the macroscopic properties of the sample, such as temperature, pressure, and concentration [3]. The Beer-Lambert law can be described by equation (2.4)

$$T_\nu = \frac{I_t}{I_0} = \exp(-\alpha) = \exp(-PS(T)\phi_\nu \chi_i L) \tag{2.4}$$

where the transmittance, T_ν, is the ratio of the transmitted intensity, I_t, and incident intensity, I_0, that is equivalent to the exponential of the negative of the spectral absorbance, or optical depth (OD), α. As light travels through a medium, in this case a gas, a fraction of the light is absorbed depending on the light's wavelength and the optical transition of the species in the medium [9]. The optical depth is a dimensionless parameter that determines how much is absorbed based on the product of the sample's static pressure, P, line strength, $S(T)$, line shape function, ϕ_ν, mole fraction of the absorbing species, χ_i, and the path length, L as shown in equation (2.5). The optical depth is the natural logarithm of transmittance, T_ν, and is commonly plotted as a function of the wavenumber to create what is known as an absorption spectrum. The absorption spectrum is a measure of a signal's attenuation through a medium and represents the transitions between energy states based on the interactions between electromagnetic radiation and the absorbing species [3]. These transition lines are

usually represented by their peak wavenumbers and contain information on the macroscopic properties of the sample, such as temperature, pressure, and species concentration.

$$\alpha = -PS(T)\phi_\nu \chi_i L \tag{2.5}$$

The line strength, $S(T)$, is a determination of the incident frequency's ability to excite the electrons through induced absorption. It is a function of the gas temperature, T, and is given by (2.6)

$$S(T) = S(T_0)\frac{Q(T_0)}{Q(T)} \exp\left[\frac{-hcE''}{k}\left(\frac{1}{T} - \frac{1}{T_0}\right)\right] \times \frac{\left[1 - \exp\left(\frac{-hc\nu_c}{kT}\right)\right]}{\left[1 - \exp\left(\frac{-hc\nu_c}{kT_0}\right)\right]} \tag{2.6}$$

where $S(T_0)$ is the line strength of the HITRAN referenced temperature, $T_0 = 296$ K, $Q(T)$ and $Q(T_0)$ are the rovibrational partition functions, h is Planck's constant, c is the speed of light, E" is the lower energy state, k is the Boltzmann constant, and ν_c is the line center frequency [2, 3, 9, 10].

The line shape is a function of temperature, pressure, composition, and line broadening mechanisms. For pressures at about 1 atm, the line shape is usually well approximated by the Voigt profile [11]. The Voigt profile is a spectral line shape that results from the collisional and Doppler broadening mechanisms resulting from the convolution of the independent Lorentzian and Gaussian functions, respectively [3, 10, 12]. Therefore, the line shape is given by (2.7)

$$\phi_\nu = \frac{1}{\alpha_D}\sqrt{\frac{ln(2)}{\pi}} K\Big(\frac{(\nu - \nu_0)}{\alpha_D}\sqrt{ln(2)}, \frac{\alpha_D}{\alpha_L}\sqrt{ln(2)}\Big) \tag{2.7}$$

where α_D is the Doppler width, α_L is the Lorentz width, ν is the incident wavenumber, ν_0 is the transition line center wavenumber, and K is the Voigt function. Because the Voigt profile is a convolution of the normalized Gaussian and Lorentz profiles, the line shape function ϕ_ν is normalized such that integrating over the frequency or wavelength yields a value of unity as shown in equation (2.8).

$$\int_{-\infty}^{\infty} \phi_\nu d\nu = 1 \tag{2.8}$$

Therefore, integrating the Beer-Lambert Law (2.4) over $d\nu$ from -∞ to +∞ yields

$$A_i = \int_{-\infty}^{\infty} -ln(T_\nu)d\nu = PS_i(T)\chi_\nu L \tag{2.9}$$

where A_i is the area of the integrated absorbance [3, 10].

For two-line thermometry, the integrated absorbances of two transitions are measured simultaneously with the same total pressure, P, mole fraction, χ_ν, and path length, L, and can be expressed as a ratio. The ratio of the two integrated absorbances will then simplify to the ratio of the line strengths, $S_i(T)$ as shown in equation (2.10) [3, 5, 10, 13].

$$\frac{A_1}{A_2} = \frac{S_1(T)}{S_2(T)} = \frac{S_1(T_0)}{S_2(T_0)} \exp\left[\frac{-hc}{k}(E_1'' - E_2'')(\frac{1}{T} - \frac{1}{T_0})\right] \tag{2.10}$$

This equation can then be used to solve for the gas temperature, T, as shown in the following equation (2.11) [3, 5].

$$T = \frac{(\frac{hc}{k})(E_2'' - E_1'')}{ln\frac{A_1}{A_2} + ln(\frac{S_2(T_0)}{S_1(T_0)}) + (\frac{hc}{k})(\frac{E_2'' - E_1''}{T_0})} \tag{2.11}$$

Once the temperature has been determined, the mole fraction of the absorbing species, χ_i, can be found using a variation of the ideal gas law (2.12).

$$\chi_i = \frac{N}{\frac{n_A P}{RT}} \tag{2.12}$$

where N is the number density of the absorbing species, n_A is Avogradro's number, P is the static pressure, R is the universal gas constant, and T is calculated gas temperature.

Chapter 3

Setup and Experimentation

3.1 Line Selection and Spectral Databases

The diagnostic process begins by identifying a spectral region for the species of interest. Selecting the appropriate spectral region is primarily based on line strength, lower energy state level, temperature sensitivity of the species' absorption transitions, and wavelength accessibility [14]. As referenced in equation (2.6), line strength is dependent on temperature and must contain transitions that are strong enough to provide proper absorption, but not so much so that the signal is completely absorbed. Recall for two-line thermometry, the gas temperature can be derived by taking the ratio of integrated absorbances, which is the ratio of the two line strengths as referenced from equation (2.10). It is recommended that the individual lines contain largely different lower state energy levels, E'', so that the ratio of integrated absorbances can derive an accurate temperature measurement. As a general rule, the greater the difference between the two lower energy states, the greater the temperature sensitivity. It is also important to select lines that are relatively isolated from each other. Lines that overlap with strong lines of other combustion species can increase uncertainties during analysis. Last but not least, the transitions of interest must be accessible by commercially available lasers [5]. All of these parameters that determine the appropriate line selection can be referenced through the use of spectral databases.

Spectral databases are used extensively throughout the TDLAS diagnostic process as they provide important information on proper line selection as well as data to simulate absorption

spectra for the samples of interest [11]. Many of the variables from Section 2.2, such as spectral line position, line strength, lower state energies, pressure-broadening, etc., can all be referenced from spectroscopic databases such as HITRAN or HITEMP [12, 15]. High-Resolution Transmission Molecular Absorption, or HITRAN [16], is a compiled database that was developed in the early 1970s for spectral parameters of known gas properties that are commonly found and used in atmospheric conditions. This, however, leads to absorption lines at elevated temperatures to become inaccurate outside of atmospheric conditions. In an attempt to alleviate this issue, another spectroscopic database, the High-Temperature Molecular Spectroscopic, or HITEMP [17], was developed in 1995. Much like HITRAN, HITEMP provides line information but only for absorbers commonly found in combustion products such as H_2O, CO_2, CO, NO, and OH. While they provide much useful information, spectral databases are known to contain incorrect line information as well as missing or additional line features at higher temperature [9]. It is recommended that experimental results are validated with lines for mixtures of known temperature and species concentration in order to circumvent this issue [2].

Windows Optical Spectra Code, or WinOSC, is a code written by researchers at Arnold Engineering Development Complex (AEDC) that can create simulated spectral plots calculated from the 2010 HITRAN/HITEMP database [16, 17]. The user inputs the wavenumber range and properties of the absorbing species such as temperature, vibrational temperature, pressure, path length, velocity, and atomic and molecular species concentration. Once the program is executed, a simulated spectra plot is generated based on the user inputed conditions. In this thesis, WinOSC is used extensively throughout the diagnostic process to model and compare spectra.

3.2 UTSI Spectroscopy Lab

In laser absorption spectroscopy, a lab setup typically consists of a light source, sample, and detector. The light source, which is a laser at some specified wavelength, emits through the sample. The energy from the laser is absorbed by the sample if the laser's wavelength corresponds to one of the target species' unique absorption transition. The molecules in the

sample become energized from the photons from the laser and transition to a higher energy state. This change in energy will affect the intensity of the transmitted light, which is sensed by the detector and routed to a data acquisition system (DAQ) to allow macroscopic values of the sample, such as temperature and species concentration to be extracted using the Beer-Lambert Law (2.4). UTSI pairs this laser diagnostic system with a high-temperature, single-zone absorption cell, which is a sealed quartz tube that has been inserted through a tube furnace. The quartz tube is filled with test gases, e.g. either CO/N_2 or CO_2/N_2 mixtures, and tested at different known gas concentrations and temperatures. The spectra generated from these results are compared to simulated spectra to test how accurately the laser diagnostic system can be used to measure species concentration and temperature based on spectral databases.

3.2.1 Laser Measurement and Detector Setup

Lasers have become a popular tool used in combustion diagnostics based on their nonintrusive nature and fast response time [2]. The purpose of the lasers is to tune across the species' unique frequency of absorption and energize the atoms into a higher energy level. Because each species has its own unique frequencies of absorption, they will have their own unique absorption spectrum that can be used to identify the composition of the species. Tunable diode lasers (TDL) have become the preferred laser source in combustion diagnostics since their development in the early 1970s. TDL have gained popularity due to their availability and affordability as well as their ability to probe the mid-infrared in spectral bands most common to combustion products. These lasers take the path-averaged measurements along the line-of-sight and provide fast response times as well as effective time-resolved, in situ measurements [5, 18]. The UTSI system features two different types of tunable lasers: a quantum cascade laser (QCL) at 5.16 μm and a distributed feedback laser (DFB) at 2.74 μm. The QCL is used for CO and H_2O measurements while the DFB is used for CO_2 measurements. These lasers produce a monochromatic frequency that is tuned across the species' absorption lines by adjusting the current or temperature of the laser [11]. Both lasers run simultaneously during testing to perform a sweeping measure over the line-of-sight. Along the laser's path are mirrors and an optical filter that are carefully

aligned to maximize the voltage strength of the photodetectors. Each laser also features its own photodetector to detect the attenuation of the laser caused by the absorbing species. An optical filter is used to diverge the beams to their respective detectors. The DFB laser uses an Indium-Antimonide photodetector while the QCL uses a Mercury Cadmium-Telluride photodetector. Figure 3.1 shows a diagram of the setup of UTSI's laser diagnostic system [2]. The optical breadboard on the left mounts the laser system while the one on the right mounts the detectors. The test gas section in the center is where the absorption cell is located.

Laser spectra for 5.16 μm and 2.74 μm associated with the lasers in the experiment were simulated for concentrations of 3% CO, 1% CO_2, and 1.9% H_2O as shown in Figure 3.2. These concentrations were selected because they are the concentrations used in the experiments. A uniform temperature of 1173 K, pathlength of 70 cm., and pressure of 1 atm were assumed for this simulation. The 5.16 μm laser has a sweep range between the wavenumbers 1937.2 cm^{-1} and 1938.3 cm^{-1} and is used to detect CO and H_2O absorption lines. Based on the simulation, there is one strong CO line at roughly 1937.8 cm^{-1} and two strong H_2O lines at approximately 1937.45 cm^{-1} and 1937.95 cm^{-1}. The presence of CO_2 is not detected within this spectral region. Another simulation was performed for the 2.74 μm laser under the same conditions whose sweep range is between the wavenumbers 3632.8 cm^{-1} and 3633.3 cm^{-1}. This region contains only one strong CO_2 line at roughly 3633.055 cm^{-1}. There is a small H_2O line at about 3632.85 cm^{-1}, but this line is small enough to be negligible. The presence of CO is not detected within this spectral region.

3.2.2 High Temperature Absorption Cell Setup

The University of Tennessee Space Institute uses a high-temperature, single-zone absorption gas cell for testing and calibration of combustion products (see Figure 3.3). The setup features a Carbolite® tube furnance, model number TZF 12/38/400, with three heating zones and a maximum operating temperature of 1200°C. Tube furnaces provide stable testing environments over extended periods of time, but they suffer from nonuniform temperature distributions and low maximum temperatures. Combusting flows can reach up to temperatures that are double the maximum temperature of the current UTSI furnace, so

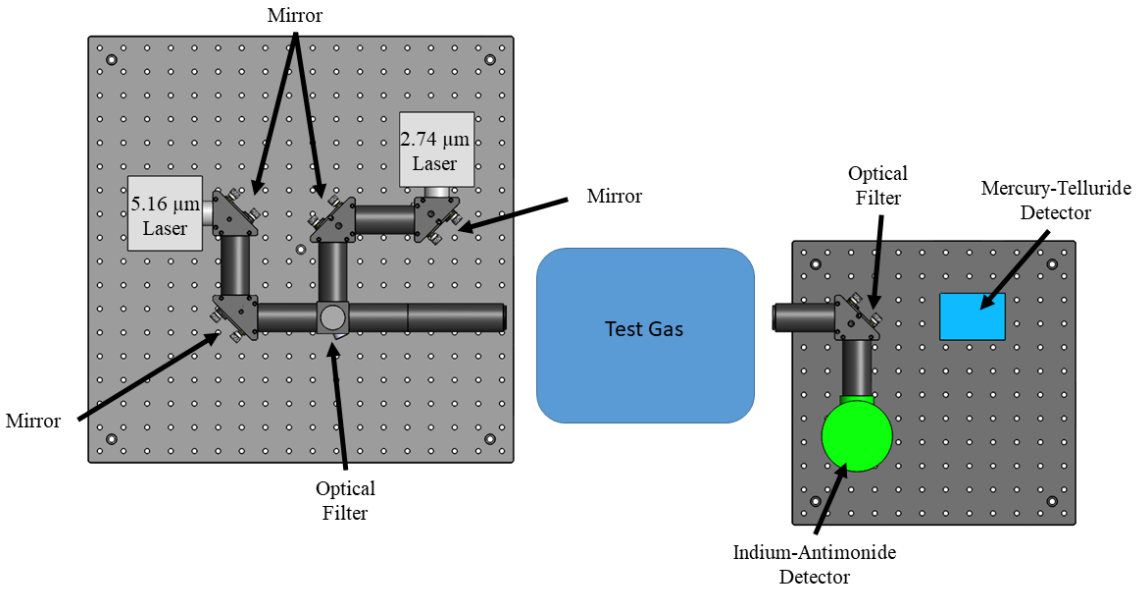

Figure 3.1: Schematic of UTSI's TDLAS setup drawn by Katrina Sweetland [2]. The optical breadboard on the left mounts the laser system while the one on the right mounts the detectors. The test gas section in the center is where the absorption cell is located.

testing at higher temperatures is desired in order to simulate the flow conditions. However, testing at higher temperatures is limited by the melting point of the materials used in the test cell. Many high-temperature metal alloys are unable to withstand the high temperatures realized in combustion environments, and the ones that can, such as rhenium, Inconel, and Haynes, are expensive and hard to machine/fabricate. Therefore, many absorption cells feature high-temperature, glass materials, such as quartz, sapphire, or alumina, in the hottest regions [3, 7, 19].

Quartz has a maximum operating temperature up to 1200°C and can be easily fabricated at low costs [20]. In the current absorption cell, a 68.5 cm. long quartz tube with an outer diameter of 3.56 cm. and an inner diameter of 2.92 cm. is positioned through the center of the furnance. The quartz tube extends about 10.5 cm. on each side of the furnace and is supported by 7.62 cm. stainless steel flanges mounted on a post. Kalrez O-rings are placed between the flange parts to create a seal. The flanges feature an inlet/outlet port that allows the test gases to enter and exit the quartz tube. The flanges also seat a 2.54 cm. diameter

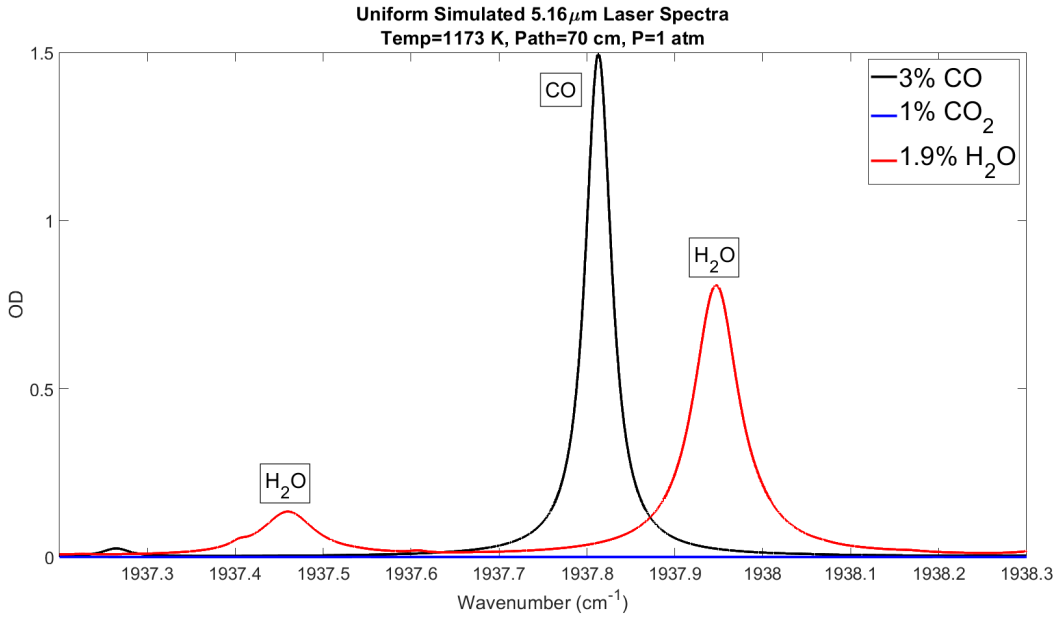

(a) Simulated spectra for 3% CO, 1% CO_2, and 1.9% H_2O between the sweep range 1937.2 cm^{-1} and 1938.3 cm^{-1} for the 5.16 μm laser.

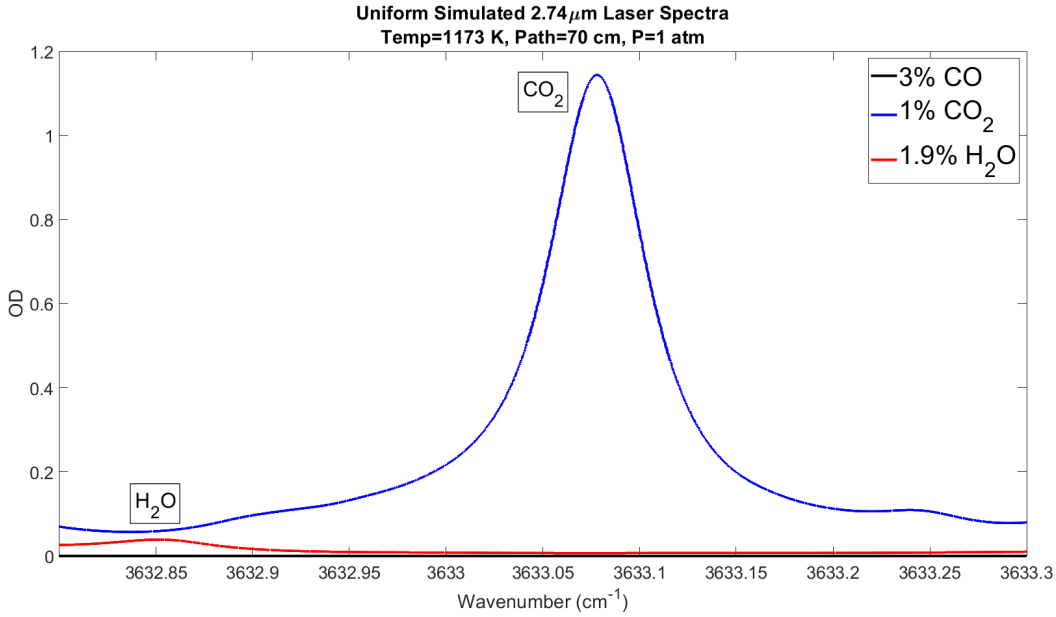

(b) Simulated spectra for 3% CO, 1% CO_2, and 1.9% H_2O between the sweep range 3632.8 cm^{-1} and 3633.3 cm^{-1} for the 2.74 μm laser.

Figure 3.2: WinOSC simulated spectra for 3% CO, 1% CO_2, and 1.9% H_2O for the 5.16 μm and 2.74 μm laser.

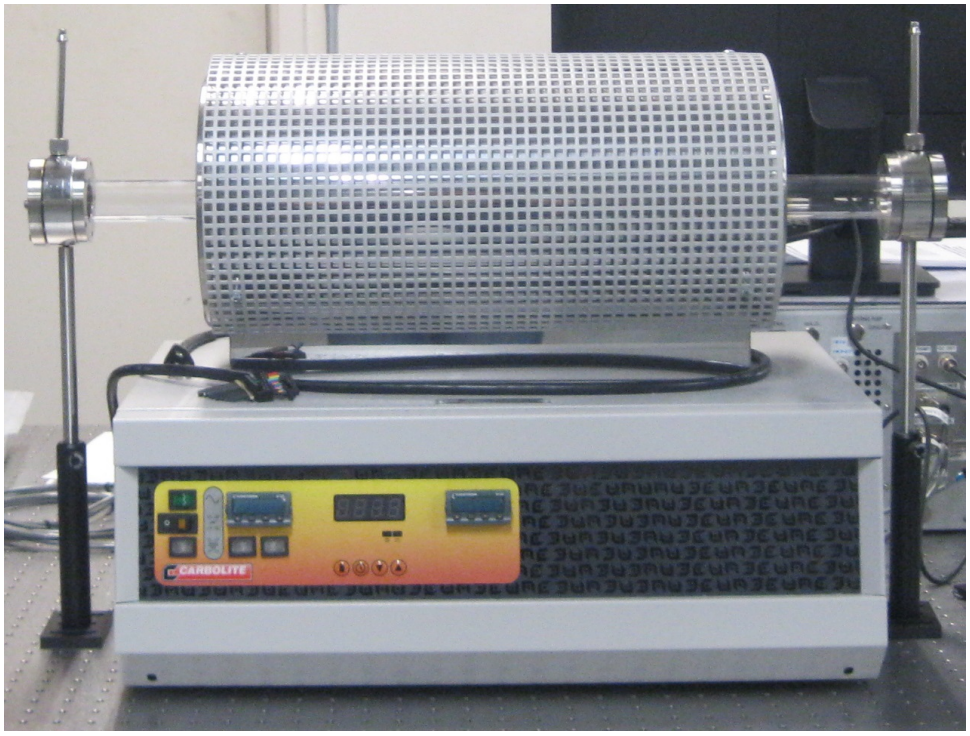

Figure 3.3: UTSI's Carbolite ® tube furnace with a quartz tube placed through the center and supported by steel flanges.

sapphire window (Al_2O_3) with a 1.5° bevel and a Teflon ring with the same diameter and bevel to seal the quartz tube and serve as an optical filter for the lasers. When selecting the window material, it is important that the materials remain transparent and nonreactive at high temperatures. Sapphire is completely inert to air, CO, CO_2, H_2O, and NO, and blocks the transmission of electromagnetic radiation for wavelengths approximately greater than 6 μm thus restricting the wavelength range to bands of interest for the species being studied [7]. It is also very durable, which allows it to be fabricated into small thicknesses of several millimeters minimizing the absorption losses.

The single-zone absorption cell design is a simple and inexpensive option when conducting spectral studies in the mid-infrared, but the major drawback is that the test gases are subjected to temperature nonuniformities near the end of the cell. TDLAS takes the path-averaged value of its measurements and is problematic if nonuniformities exist along the laser's line-of-sight. Typically, line-of-sight measurements have been limited to flowfields with uniform temperature and species concentrations, so nonuniformities will affect the accuracy of the measurements. However, uniform flowfields rarely exist in practical combustion

applications due to flow mixing, chemical reactions, phase changes, and heat transfer effects; therefore, corrective techniques, such as profile fitting, temperature binning, tomographic reconstruction, and boundary layer corrections, have been developed to reduce the effects that nonuniform conditions have on the results [5, 13, 21]. Heating tapes, band heaters, conductive cell materials, and thermal insulatation are other solutions people have used to address the temperature gradient. The absorption cell at UTSI suffers from temperature nonuniformities. The ends of the quartz tube are exposed to room temperature creating a large temperature gradient in that area introducing uncertainty into calibration experiments. A potential solution to the temperature gradient issue is to design and develop a three-zone absorption cell.

3.3 Proposed Three-Zone Absorption Cell Design

The University of Tennessee Space Institute is planning to replace the current high temperature absorption cell to a proposed three-zone absorption cell based on a design by the Technical University of Denmark [3, 7]. A variation of this design [3], as shown in Figure 3.4, was suggested as a solution to allieviate the effects of the high temperature gradients found in the current absorption cell by creating chambers in the nonuniform regions and filling them with nitrogen, which has negligible absorption in the mid-infrared at combustion temperatures. Along with the nitrogen chambers, the proposed design also features ports for thermocouples to be inserted for measuring temperature distributions during testing, which is a feature that is not possible with the current UTSI setup. The new absorption cell will use a Carbolite® STF 15/450 tube furnace with a maximum operating temperature of 1500°C. This increase in maximum operating temperature will also require new materials with higher melting points to be used in the cell. A computational model of the proposed absorption cell was created to validate and verify the maximum operating temperature of the new design. For more information on the proposed cell model and its simulations, the reader should reference Mr. Travis Johnson's thesis [3].

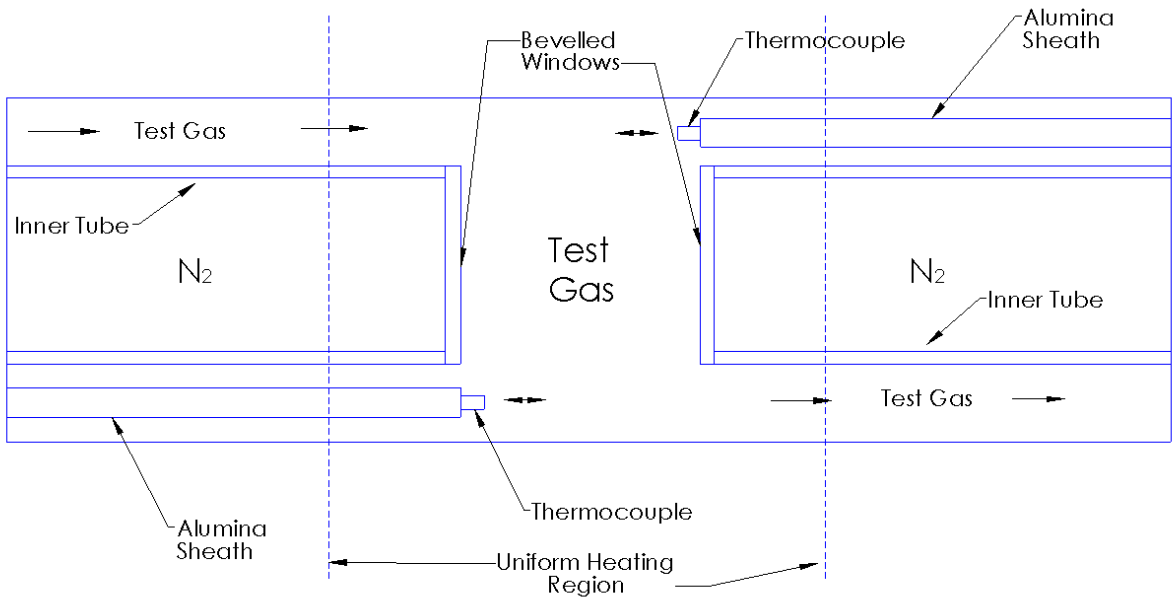

Figure 3.4: Drawing of the proposed three-zone cell design by Travis Johnson. [3].

3.4 Thermal Insulation

While Mr. Johnson's design is a solution to the temperature nonuniformity problem, UTSI, at the time of writing this thesis, is currently in the process of securing funding for this project. Instead, a temporary solution proposed is to insulate the exposed ends of the quartz tube with ceramic fiber blankets to help assess the effects of the high temperature gradients. Insulating the ends of the furnace will slightly reduce the temperature gradient, but it is not supposed to be a permanent solution, nor will it eliminate the nonuniformities. While other options provided more viable results, they were either too expensive or unfeasible with the current cell design. Because plans and funding for the three-zone absorption cell were already in the works, the author did not want to expend major funds to a project that would soon be outdated. Fortunately, the ceramic fiber blankets were available to the author at no expense. The purpose of applying the insulation is to study the degree to which a lower temperature gradient will reduce the uncertainty of the LOS measurements through comparison with simulated results. The insulating material is a MaxWool^{TM} HPS ceramic fiber blanket (Figure 3.5) woven from a blend of alumina and silica material. Ceramic

Figure 3.5: MaxWool^{TM} HPS ceramic fiber blanket used to insulate the quartz ends of the tube furnace.

fiber blankets have a low thermal conductivity and are commonly used as insulation for high temperature applications such as heat shields, boiler insulation, and industrial furnace lining. The blanket is 1" thick with a density of 8 lb/ft^3 and a maximum operating temperature of 1350°C [22]. The blankets are wrapped around the exposed ends of the quartz tube and held together with foil tape as shown in Figure 3.6.

3.5 Temperature Distribution Tests

The current UTSI system does not allow taking real time temperature distribution measurements while test gases are flowed through the system. Therefore, axial temperature measurements of the tube furnace are performed in air under static conditions with a K-type thermocouple in order to verify the temperature distribution along the line-of-sight. A slide rail with an arm was designed to mount a K-Type thermocouple, as shown in Figure 3.7, so that it could traverse through the tube furnace axially while recording its relative position with a calibrated string potentiometer. This allowed accurate measurement of the relative position of the thermocouple to within a 2% difference between the insulated and uninsulated

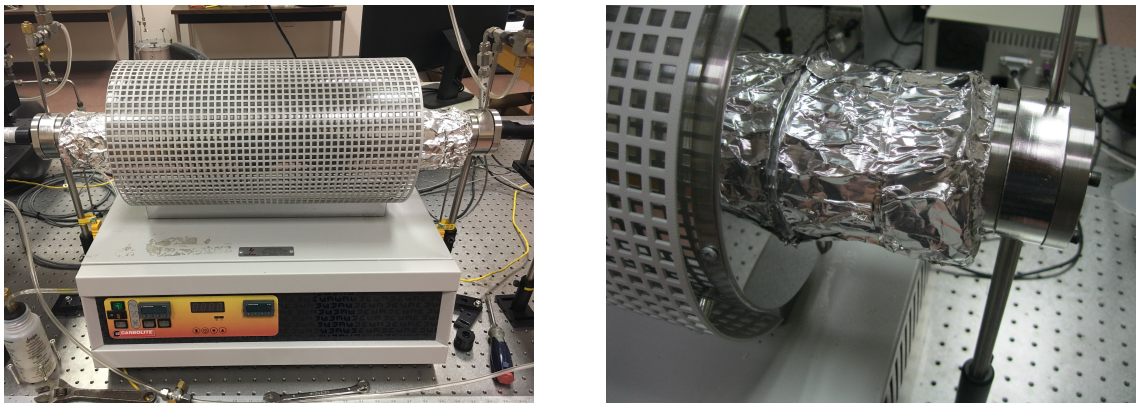

Figure 3.6: High temperature absorption cell with the quartz ends insulated with the MaxWool^{TM} HPS ceramic fiber blanket.

tube setups. The thermocouple and potentiometer were connected to a DAQ where their output were transmitted into a LabVIEW program to monitor real time measurements.

To measure the temperature profile, while facing the absorption cell, the right flange on the end of the quartz tube was replaced with a flange with an open port that allows for the insertion of the thermocouple at the tube centerline. Starting at the far right end of the flange and just outside the open port, the tip of the thermocouple was inserted roughly 35 cm. in the absorption cell and rested at the center of the furnace where the position was set as the starting point. The center was chosen because the temperature distribution of the furnace was assumed and tested to be fairly symmetric [2], so measuring one half of the furnace should yield similar results for the other half. The furnace was then set to the desired temperature where the thermocouple measured the temperature increase until it reached steady state, which was determined when the thermocouple reading stopped changing and was within a 2% difference from the furnace setting. This process normally took about an hour. Once the temperature had reached steady state, the thermocouple was slowly backed out in 1.27 cm. intervals measuring the local temperature. Each measurement was taken when the change in temperature from the thermocouple was less than 1% per minute. This process normally took 15-20 minutes per interval.

Temperature distribution tests were performed for insulated and uninsulated quartz ends for furnace settings of 250°C [523.15 K], 500°C [773.15 K], 750°C [1023.15 K], and 900°C [1173.15 K]. While 1200°C is the maximum operating temperature of the furnace, testing

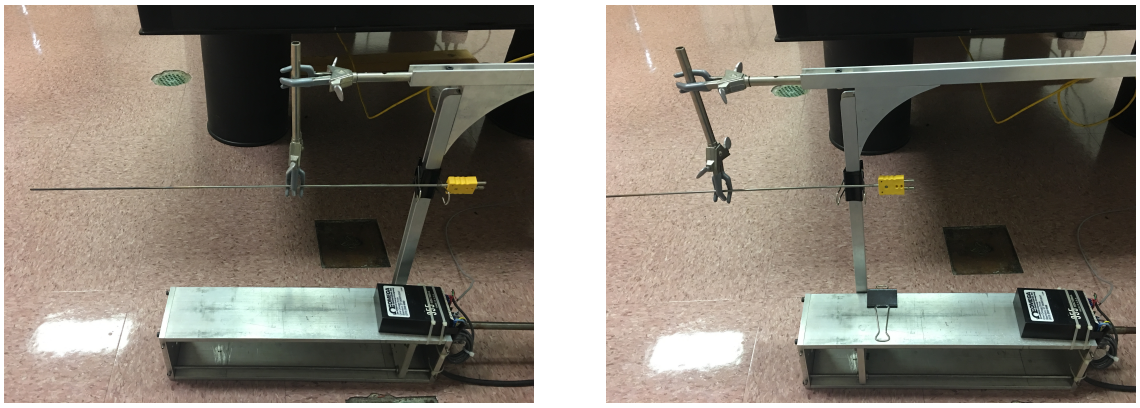

Figure 3.7: A slide rail with an arm designed to mount a K-type thermocouple for axial temperature measurements through the tube furnace.

conditions did not exceed 900°C due to the temperature limitations of the o-rings within the absorption cell flanges. Two K-type thermocouples were secured on the flange posts and used to monitor the flange temperature. During temperature distribution tests for uninsulated ends at 900°C, the o-rings were observed to be glowing red from the high temperatures, which placed a concern that the o-rings were nearing their maximum operating temperature of 232 °C. Insulating the ends would only increase the temperature in that region, so thermocouples are used to monitor the increase in flange temperature to ensure that the o-rings do not exceed their operating conditions. Based on the temperature distribution plot in Figure A.4 of the furnace's half profile, a temperature of roughly 200°C was recorded around the o-rings, which is slightly below their maximum operating temperature. 900°C is therefore selected as the maximum furnace setting for the experiments.

Figure 3.8 is the result of the temperature distribution test for a furnace setting of 900°C. Although half the absorption cell was measured, a full cell distribution was plotted by mirroring the results because the temperature distribution of the furnace is assumed to be symmetric. Table A.10 tabulates the measured temperatures and shows the percent change between insulation versus no insulation. The absorption cell's temperature maintains good uniformity mostly throughout the center of the furnace but begins to decline about 7.62 cm. from the end of the furnace. The decline around that position is apparent in the other temperature distribution tests as well. For 900°C, the effects of the insulation are most prominent as the furnace temperature increases showing up to a 120% increase compared to

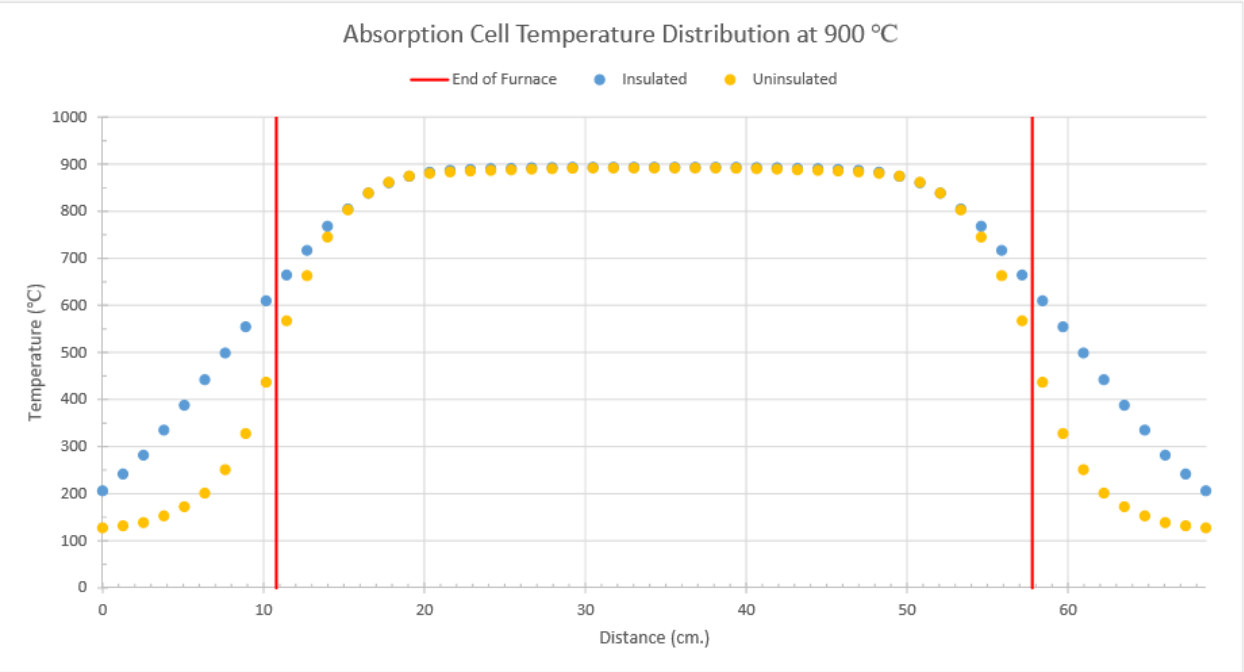

Figure 3.8: Full profile temperature distribution of the absorption cell at furnace setting of 900°C.

its uninsulated counterpart at that position. While the insulation does alleviate much of the steep temperature gradient, large nonuniformities still exist in the system. It was hoped that the insulation would extend the uniform temperature region within the furnace, but instead it only raises the temperature of the exposed cell region. The results of the temperature distribution tests can also be referenced in Appendix A.

Using the results from the temperature distribution tests, a simulated spectra can be created to predict the spectra for a nonuniform temperature distribution. WinOSC is capable of superimposing up to 10 spatial layers to create one model, which allows the user to divide a non-homogenous optical path into 10 homogenous sections. However, there are more measured points than there are available layers, so the points must be divided into at least 10 layers with each layer taking the average of the measured temperature points. Because the temperature distribution is assumed to be fairly symmetric, the half temperature profile was used to decrease the number of temperature points averaged per layer so that a more accurate result could be simulated. Note that the optical density of the absorption spectrum will later have to be doubled to adjust for the half-profile measurement. In the simulation discussed

in subsequent sections, it is assumed that temperature is the only changing variable and that species concentration and atmospheric pressure are constant for all layers. Vibrational temperature is kept as 0, and the velocity is 0 because the gas in the cell is stagnant.

Starting from the furnace center and measuring outwards toward the flanges, K-type thermocouples measured the cell temperature to be roughly 2% of the set furnace temperature of 900°C for about 10 cm. from the centerline for both insulated and uninsulated conditions. This 10 cm. section is used for the first layer and assumed to be a uniform temperature. Beyond this point, the temperature distribution would drastically deviate from the set furnace temperature by as much as 3 - 77%. Eight layers were created for the remaining temperartures with two temperatures points averaged for each layer. The path length of each layer was calculated by taking the difference of locations between the two measured temperatures. Nine uniform layers were created, and Tables A.11 and A.12 tabulate the values used for each layer for the uninsulated and insulated temperature distributions, respectively, at a furnace setting of 900°C [1173 K]. A plot of how the layers are matched to their corresponding half-temperature profiles is shown in Figure A.4, where the dashed lines are the layers and the triangles are the thermocouple measurements. The results of the temperature distribution tests for 250°C [523.15 K], 500°C [773.15 K], and 750°C [1023.15 K] can be referenced in Appendix A.

3.6 Absorption Cell Testing

Before the gas is flowed through the absorption cell, it must first be premixed to desired, known concentrations in a separate tank, as referenced in Figure 3.9, using Dalton's Law of Partial Pressures (3.1)

$$P_i = (\chi_i)P_T \tag{3.1}$$

which states that partial pressure, P_i for species i is equivalent to the species mole fraction, χ_i multiplied by the total pressure of the gas mixture, P_T. A total gas mixture of 50 psia was used for these experiments with concentrations of 3% CO/97% N_2 and 1% CO_2/99% N_2.

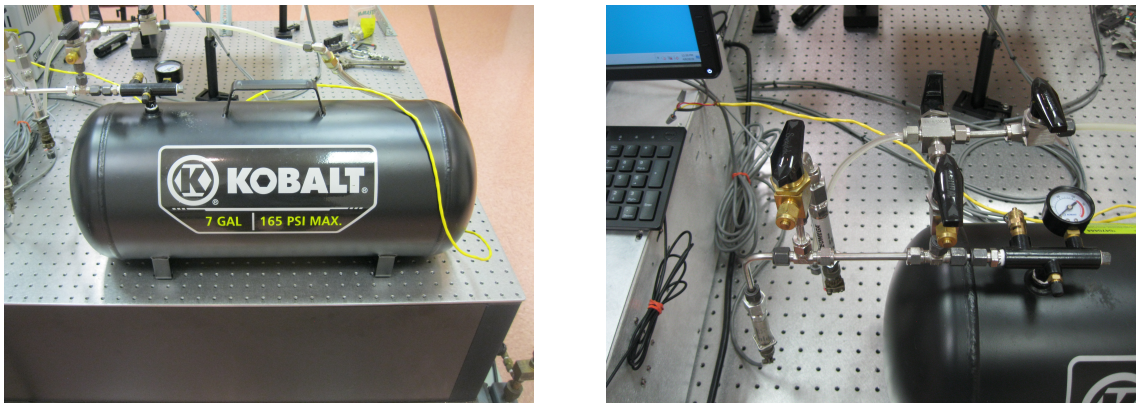

Figure 3.9: An air tank was used to premix the gases to desired concentrations using Dalton's Law of Partial Pressures. Valves and pressure transducers were used to control and monitor the gas pressure during premixing and absorption cell testing.

With these values known, the partial pressure required to achieve the desired concentrations was calculated to be 1.50 psia of CO and 0.5 psia of CO_2.

Before premixing the gases, the contents of the tank were purged and subjected to vacuum using a mechanical vacuum pump. The tank was then backfilled to roughly 15 psia of nitrogen where it was once again purged and subjected to vacuum. This process was done at least three times in order to remove as many impurities as possible remaining in the tank. Once the purging process was complete, the mixing process begins by filling the tank with the lowest concentration in the mixture, which was either CO or CO_2, depending on which test was being performed. The remainder of the tank was filled with nitrogen until the absolute pressure of the tank reached the total pressure required to achieve the desired mixture concentration. One issue with this procedure is that an accurate concentration was reliant on how well the experimentalist was able to achieve the desired pressures based on the pressure transducer readings, which was known to fluctuate and vary by as much as +/- 1 psi. Once the gas was premixed, it sat for approximately 5 minutes to allow the gas to come to uniformity. More gas was then added as needed. After premixing, there was no other way to confirm the mixture concentration. A detailed mixing procedure can be referenced in Appendix B.

The absorption cell must also be purged of impurities. The inlet and outlet valves on the absorption cell were opened, and the nitrogen bottle was then attached to the inlet of

the absorption cell and was used to purge the cell by allowing the gas to flow through for approximately 3 minutes. Once this process was complete, the valves on absorption cell were closed and the nitrogen line was detached from the absorption cell and hooked to the laser and detector setup where it then purged the laser and detector system throughout the remainder of the experiment, reducing the absorption of the laser's path outside of the absorption cell due to air absorption. The tank with the premixed gases was attached to a water bubbler, which is a sealed bottle partially filled with tap water. The gas from the tank gently flowed into the water to create bubbles, and the flow exited the bubbler through an outgoing line that was above the water. The outgoing line is attached to the inlet flange on the absorption cell, where it was now ready to fill the test cell. This process was required because water must be present within the gas mixture for the proper operation of the data reduction program associated with the TDLAS instrumentation to calculate the species temperature from the ratio of the H_2O lines.

The furnace was then turned on and data was ready to be collected, starting with the lowest temperature, for furnace temperature settings of 250°C, 500°C, 750°C, and 900°C. Valves and a pressure transducer were used to control and monitor the test cell so that it maintained a pressure of slightly above 1 atm. A positive pressure was maintained throughout the cell to prevent the atmosphere from leaking into the cell. Since gas expands when heated, the pressure inside the test cell increased as the furnace temperature is increased. The outlet valve on the test cell was opened to relieve the cell pressure and closed once the pressure returns to slightly above 1 atm. Once the furnace reached the desired set temperature, 60 minutes were passed before recording data to ensure that the gas was at a steady state temperature throughout the cell. While testing can be performed at different pressures, the current cell cannot exceed 25 psia before the excess pressure causes the flanges to burst from the quartz tube; therefore, a testing pressure of slightly above 1 atm was selected for these experiments.

Chapter 4

Results and Discussion

4.1 Data Collection & Post Processing

The TDLAS system manufacturer used LabVIEW to write two separate codes for collecting and processing the data obtained from the absorption cell tests. LabVIEW controls the properties of the laser, records the data collected from the detectors, and is able to display a real time plot of laser voltage as a function of the sample number. After the test gases fill the test cell, the lasers are turned on. Figure 4.1 displays the signal of 3% CO in N_2 at room temperature. Detector 1 (black line) represents the reading of the Mercury-Telluride detector used for the 5.16 μm laser, and detector 2 (red line) represents the reading of the Indium-Antimonide detector used for the 2.74 μm laser. The signal's waveform is a voltage ramp where the dips in the ramp represent absorption features dependent on spectral absorbance properties of the gas. The sample number axis relates to the spectral domain where the wavenumber can be identified. When data was ready to be recorded, the DAQ was started and ran for approximately 15 seconds before saving. The data is saved in a raw format in order maintain high data rates, and the files are later exported to the post processing program for analysis.

Figure 4.2 is a plot of the voltage as a function of the sample number of the raw data taken from the Data Collection LabVIEW for 3% CO with uninsulated ends at room temperature (300 K) and furnace settings of 773 K and 1173 K. Notice that as the furnace temperature increases, the baselines on both detectors increase. The sample number does not appear to

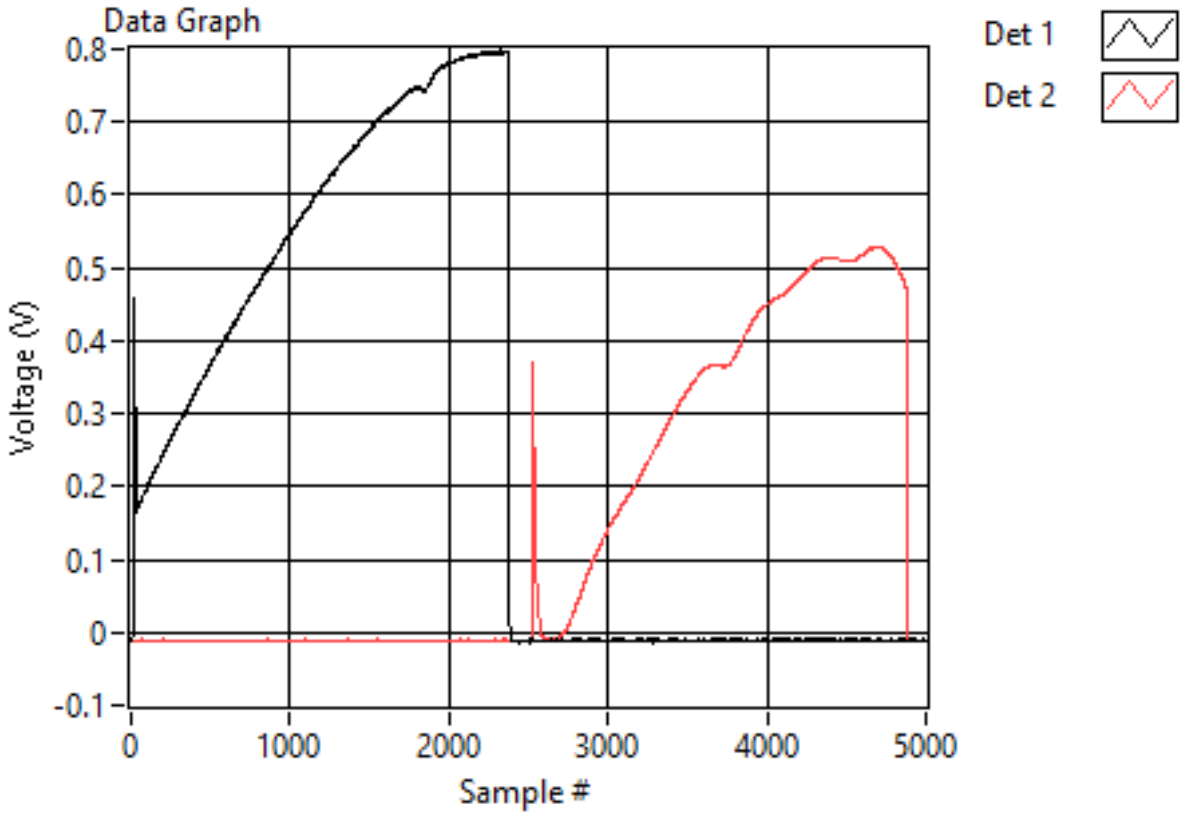

Figure 4.1: Laser sweep of 3% CO at room temperature as displayed on the Data Collection LabVIEW. Detector 1 (black line) represents the 5.16 μm laser and detector 2 (red line) represents the 2.74 μm laser.

be affected by the change in temperature; therefore, this increase in voltage in relation to the increase in temperature results in a DC offset. Because this offset is a function of furnace temperature, it will be present in all initially collected raw data regardless of the species or concentration. These DC offsets can be corrected by subtraction as seen in Figure 4.3 where the DC offset from Figure 4.2 has been corrected. Note that all subsequent raw data plots will have their offsets corrected.

The raw data itself doesn't reveal much quantitative information until it is analyzed with the post processer. However, the raw data plot is a very close resemblance of a transmission spectra with the different peaks representing the transmission of the light through a certain species in that wavenumber region. This plot is displayed by the TDLAS software and

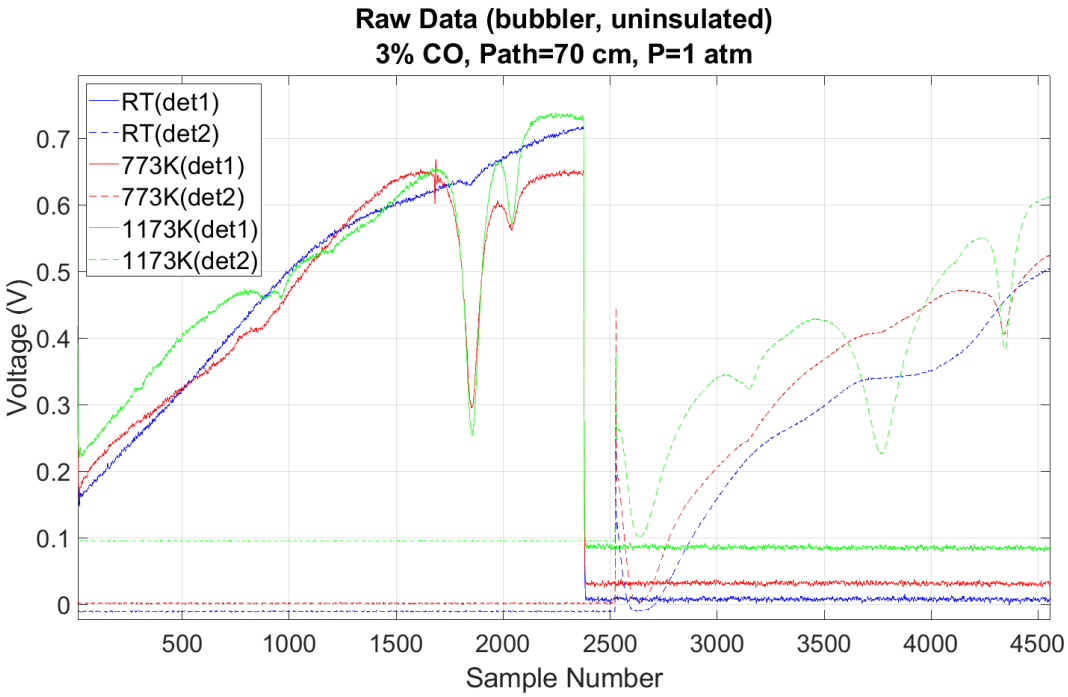

Figure 4.2: Laser sweep of 3% CO with uninsulated ends at room temperature, 773K, and 1173K as displayed on the Data Collection LabVIEW. Detector 1 (black line) represents the 5.16 μm laser and detector 2 (red line) represents the 2.74 μm laser.

allows the experimentalist to observe real time changes due to the different temperatures and concentrations in the absorption cell.

After converting the raw data to detector signal as a function of wavenumber, the post processor uses an iterative, nonlinear fit procedure to fit the data with a multipeak voigt fitting algorithm where it will extract information from the data such as peak areas, line center value for the voigt fittings, gas temperature, and the gas concentrations for CO, CO_2, and H_2O. As mentioned in Section 3.6, water must be present in the gas mixture for the post processor to accurately measure these parameters. Water has many absorption features in the spectral regions being studied, especially in the 5.16 μm laser range where strong H_2O and CO lines dominate this region. The post processor, therefore, creates a voigt fit for both the H_2O and CO lines where the ratio of the H_2O lines are used to extract the species temperature based on equation (2.11). The post processor attempts to create a voigt fit for the measured data, but this often results in the fit being placed improperly due to improper calibration, resulting in inaccurate temperature and species concentration

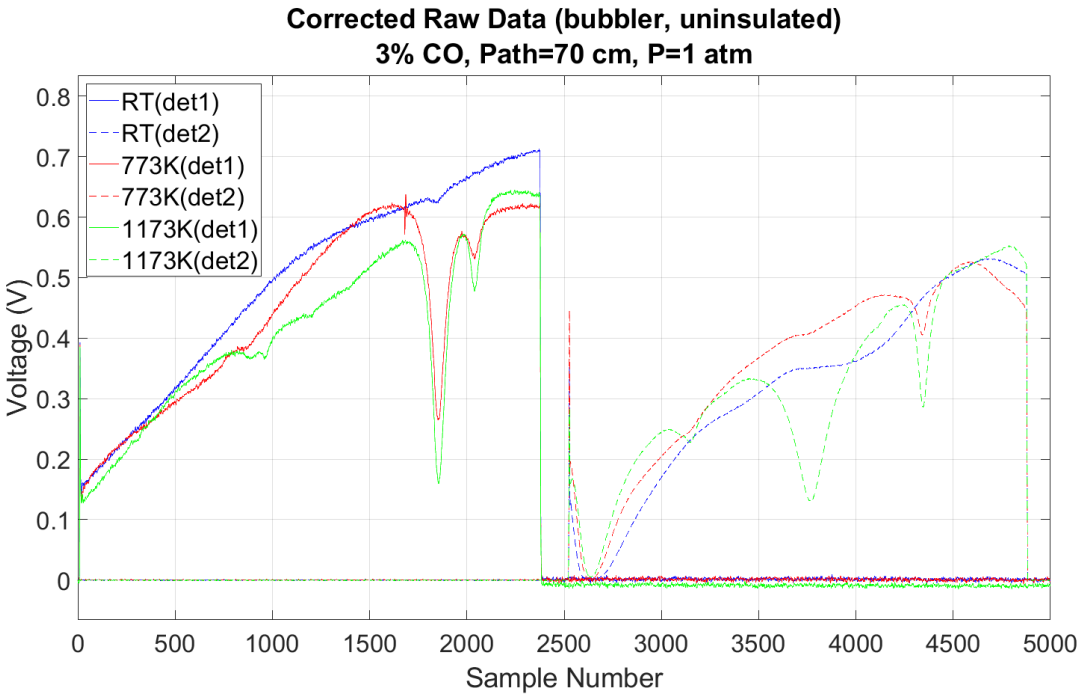

Figure 4.3: Corrected DC offset for 3% CO with uninsulated ends at room temperature, 773K, and 1173K as displayed on the Data Collection LabVIEW. Detector 1 (black line) represents the 5.16 μm laser and detector 2 (red line) represents the 2.74 μm laser.

measurements. Even with water present in the gas mixture, the post processor is unable to accurately extract temperature and species concentrations due to issues with the post processor.

Simulations from WinOSC were used to examine the absorption spectra of CO, CO_2, and H_2O at different temperatures and species concentrations. The simulated spectra could then be used to determine the appropriate concentration of the gas mixtures. Concentration is determined by optical depth of the major absorption transitions. Recall in equation (2.5) that the optical depth is a function of the gas's static pressure, P, line strength $S(T)$, line shape function, ϕ_ν, mole fraction of the absorbing species, χ_i, and path length, L. During testing, the cell pressure is kept at roughly 1.1 atm with a constant path length of 70 cm. The lineshape function is represented by the voigt profile and has nothing to do with experimental setup. The only changing variables to the optical depth are temperature and species concentration. Theoretically, the Beer-Lamber Law (2.4) ranges between 0 and 1, with 0 representing light completely passing through the sample and 1 representing light

being completely absorbed by the sample. However, experimental results do not always measure within this range. If the optical depth is too high, the light becomes greatly absorbed by the sample, increasing uncertainty error, and making it difficult to extract any useful information. Absorption that is too low results in a majority of the light passing through, also making extraction of useful information difficult. The simulations were used to model spectra for uninsulated, insulated, and uniform temperature distributions at the desired mixture concentration for furnace settings of 523 K, 773 K, 1023 K, and 1173 K. Concentrations were selected so that the optical depth measured between 0.3 and 1.5. The uninsulated and insulated spectra were modeled by superimposing multiple spectral layers in WinOSC, as shown in Section 3.5, to account for the temperature nonuniformity.

Experimental results were then compared to simulated results by comparing the fit of their absorption spectra. LabVIEW plots the measured spectra as optical depth as a function of relative wavenumber. The relative wavenumber does not display the actual wavenumber range of the absorbing species, so it had to be rescaled to match the simulated wavenumbers. The resulting experimental data were rescaled by superimposing onto the simulated data by aligning their peak features. Typically, the general line shape shared the same features as the simulated spectra, so a reference point, usually the peak wavenumber, was aligned with the peak wavenumber of the simulated spectra and the resulting plot just shifted. Unlike the simulated spectra, the measured spectra did not produce enough points to create a smooth curve; therefore, the curve fitting tool in MATLAB was used to estimate the curve profile based on a Gaussian fit. A Gaussian fit was selected as it was the only fit projection in the MATLAB curve fitting tool that best fit the data considering the voigt profile is a convolution of a Gaussian and Lorentzian profile. Statistical values generated by the curve fitting tool determined how well the Gaussian curve fits the measured data for the insulated and uninsulated tests, respectively.

The statistical parameters that can be used to assess line comparisons are the sum of squared errors (SSE), R-Square, and Root Mean Squared Error (RMSE). The SSE, eqn. (4.1), measures the total deviatation of simulated data to that of the measured data where an SSE that approaches 0 indicates a good fit between measured values and the fitted curve. The SSE is determined by taking the sum of the squared difference between measured points,

y_i, and the predicted value, $\hat{y}$, for all data points, n. The R-Squared value, eqn. (4.2), ranges from 0 to 1 and is a measure of how well the variance is represented by the fit. It can be viewed as a percentage with an R-Squared of 1 indicating the model fits 100% of the measured data. The R-Squared value is determined 1 minus the ratio of SSE to the sum of squares total (SST), where y_i is the measured value, $\hat{y}$ is the predicted value, and $\bar{y}$ is the mean value of the measured data, y. The RMSE, eqn. (4.3), is the standard deviation of the residuals. As RMSE approaches 0, this indiciates a good fit between the measured data and curve fit [23]. This value is determined by taking the square root of the ratio of the SSE to the number of data points, n.

Once the Gaussian fit was determined to be an appropriate fit for measured data, the curve fitting tool had a feature that was able to determine the fit's "goodness of validation (GOV)". The MATLAB GOV feature allowed the fitted curve to be compared with another set of data in order to determine how well their curves compared by examing their SSE and RMSE. The measured curve was compared to the simulated curve in order to assess how accurately the measured spectra was modeled by the simulated spectra.

$$SSE = \sum_{i=1}^{n} (y_i - \hat{y})^2 \tag{4.1}$$

$$R^2 = 1 - \frac{SSE}{SST} = 1 - \frac{\sum_{i=1}^{n} (y_i - \hat{y})^2}{\sum_{i=1}^{n} (y_i - \bar{y})^2} \tag{4.2}$$

$$RMSE = \sqrt{\frac{SSE}{n}} = \sqrt{\frac{1}{n} \sum_{i=1}^{n} (y_i - \hat{y})^2} \tag{4.3}$$

Finally, the simulated temperature and species concentrations were compared to temperature and species concentrations from the experiment. The simulated temperature was determined by taking the average of the thermocouple measured points from the temperature distribution tests that were used to model the simulated spectra, and the value of the known species concentration was assumed to be the desired species concentration of the gas mixture. The measured temperature and species concentrations were determined by taking the average of the temperature and concentration data points that were extracted

from the post processing software. Outliers in the data were filtered out through the modified Thompson Tau test given by equation (4.4)

$$If\ abs(x_i - mean(x)) > \tau s_x, then\ the\ data\ point\ is\ an\ outlier \tag{4.4}$$

where x_i is a data point in the data set, x, τ is constant based on the total number of data points, which in this case is 2, and s_x is the standard deviation of the data set. The modified Thompson Tau test has been used in past experiments to determine outliers from the post processing software [2]; therefore, it was selected in this test for consistency. The percent difference given by equation (4.5) was then calculated to compare the difference between the simulated and experimentally measured values. All of these parameters are examined in order to determine whether or not insulation has any effect on the accuracy of measured results, and if so, to what degree.

$$Percentage\ Difference = \frac{|Measured\ Value - Simulated\ Value|}{\frac{Measured\ Value\ +\ Simulated\ Value}{2}} \times\ 100 \tag{4.5}$$

4.2 CO Results

A spectral simulation was used to determine what effects that changing temperature and species concentration would have on the absorption spectrum of CO [1937.8 cm^{-1}] and H_2O [1937.45 cm^{-1} and 1937.95 cm^{-1}] in N_2. Although H_2O is being simulated, it is not the focus of these experiments. H_2O is present only because the TDLAS system requires water to calculate the temperature. The actual water concentration is unknown, so a concentration of 1.9% H_2O was assumed in the simulations to model the waterlines based on the results of [2]. The water concentration measured in [2] was determined from a humidifier setup with a hygrometer that extracted 0.019 mole fraction of H_2O based on a relative humidity of 73%. It is assumed that the conditions in the humidifier is similar to the conditions in the bubbler since both have similar designs, so a 0.019 mole fraction was also assumed. That experiment was designed to specifically measure temperature and species concentration of H_2O, so the

setup is slightly different than the current one. The premixed tank is replaced with with the humidifier setup to test with H_2O, but everything else is essentially the same.

Figure 4.4 shows that increasing the temperature and species concentration will increase the optical depth of both CO and H_2O. The simulation predicts CO and H_2O to have little to no absorption at room temperature. At 523 K, CO is still undetected, but the optical depth of the large water line at 1937.95 cm^{-1} shows roughly 0.3 while the other waterline at 1937.45 cm^{-1} is barely detectable with on OD of 0.01. It isn't until 773 K through 1173 K that CO and both H_2O lines can be measured with CO having an OD of 0.28 - 1.5 and the small and large H_2O lines having an OD of 0.064 - 0.14 and 0.73 - .089, respectively. The lack of water lines at room temperature and 523 K indicate that H_2O absorption is small for these lines at lower temperatures. While increasing the species concentration could potentially increase the OD to more measurable values, higher concentrations risk the spectra becoming completely absorbed at higher temperatures, as shown in Figure 4.4b, where a 5% CO concentration at 1173 K is well above the recommended OD. Disregarding room temperature and 523 K, a 3% CO concentration was selected with optical depths ranging between 0.28 and 1.53 for 773 K through 1173 K. Figures 4.5 - 4.8 compare the absorption spectra for 3% CO with uninsulated, insulated, and uniform temperature distributions at 523 K, 773 K, 1023 K, and 1173 K. The simulation shows that applying the insulation should slightly increase the optical depth, which becomes more effective at higher temperatures. Even with the insulation applied, the optical depth of a uniform condition is still more than double that of the insulated spectra.

Comparing the measured to simulated spectra of 3% CO in Figures 4.9 - 4.12, the first feature to notice is that measured optical depth is substantially greater than simulated spectra for all temperatures regardless of whether insulation was applied. This result agrees with Ref. [2], and the assumption is mainly due to the large temperature gradients. The Gaussian curves fit the measured data well with low SSE and R-Square values of 0.99 for all temperature settings. Examining the SSE (GOV) in Tables 4.1 and 4.2, the measured fits to the simulated curves are poor at low temperatures and get worse as temperature increases. Applying insulation increases the overall SSE (GOV); this is expected since increasing the temperature increases this value.

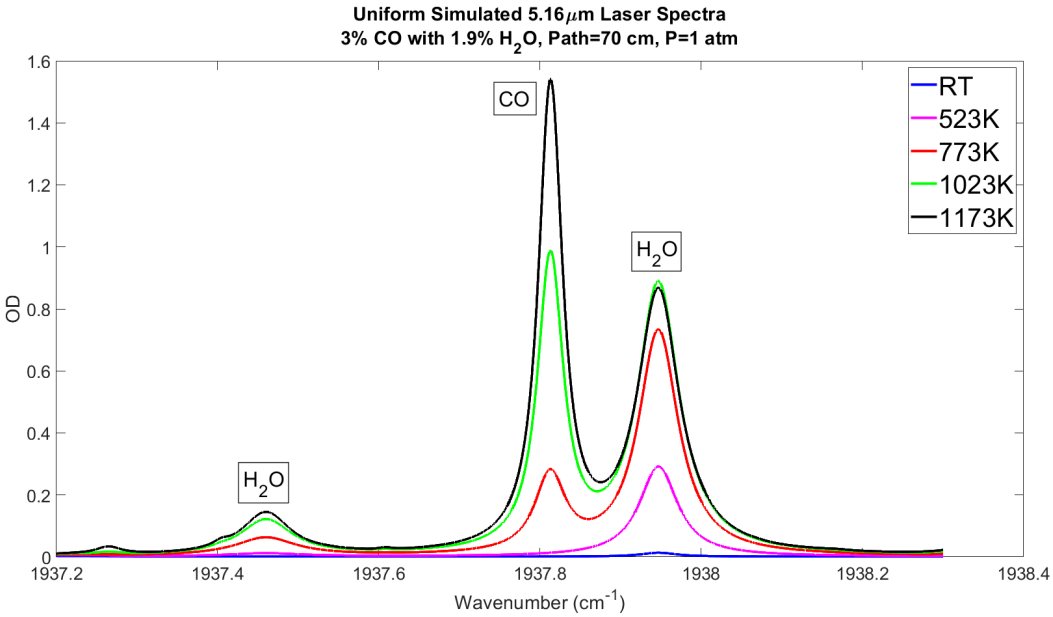

(a) Simulated spectra of 3% CO with 1.9% H_2O for room temperature - RT (27 K), 523 K, 773 K, 1023 K, and 1173 K with a path of 70 cm. and pressure of 1 atm.

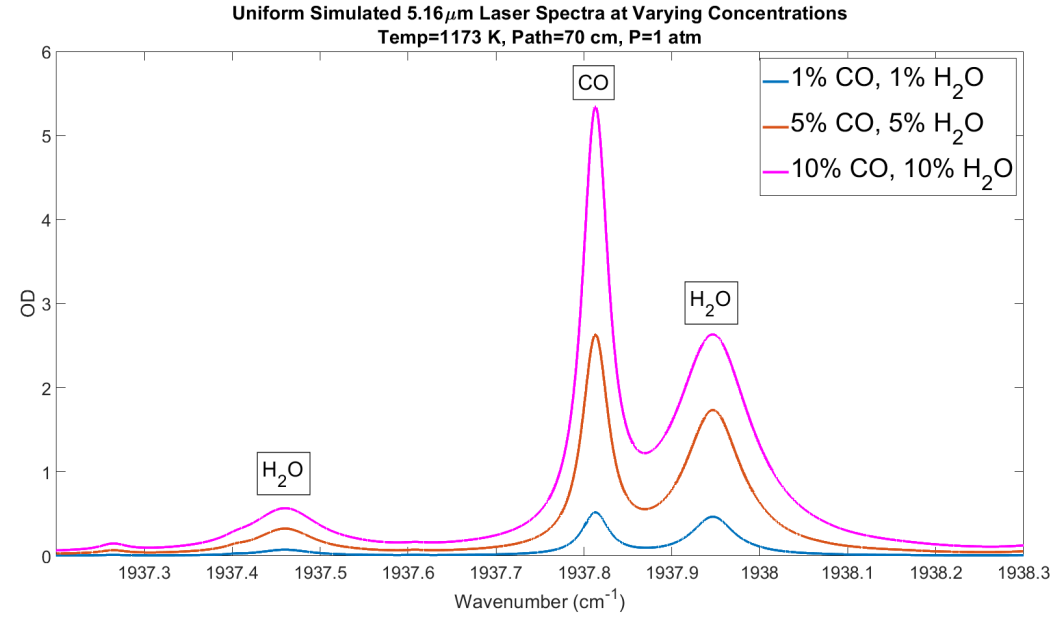

(b) Simulated spectra of 1%, 5%, and 10% CO and H_2O at 1173 K with a path of 70 cm. and pressure of 1 atm.

Figure 4.4: Simulated spectra used to examine the behavior of CO and H_2O for different temperatures and species concentrations.

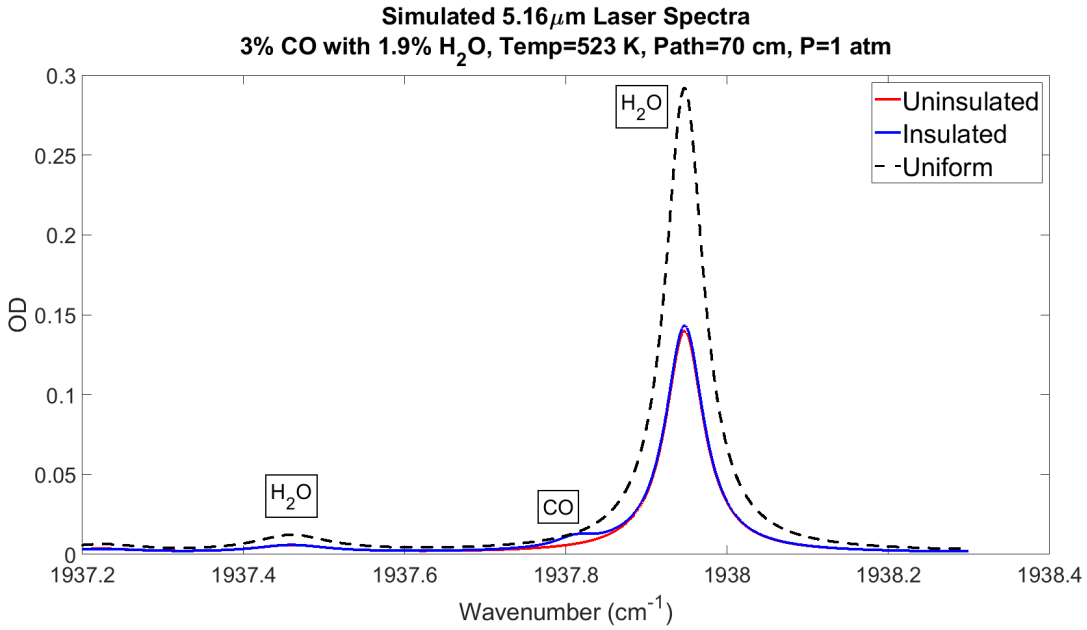

Figure 4.5: WinOSC simulated spectra for 3% CO and 1.9% H_2O at 523 K for a 5.16 μm laser.

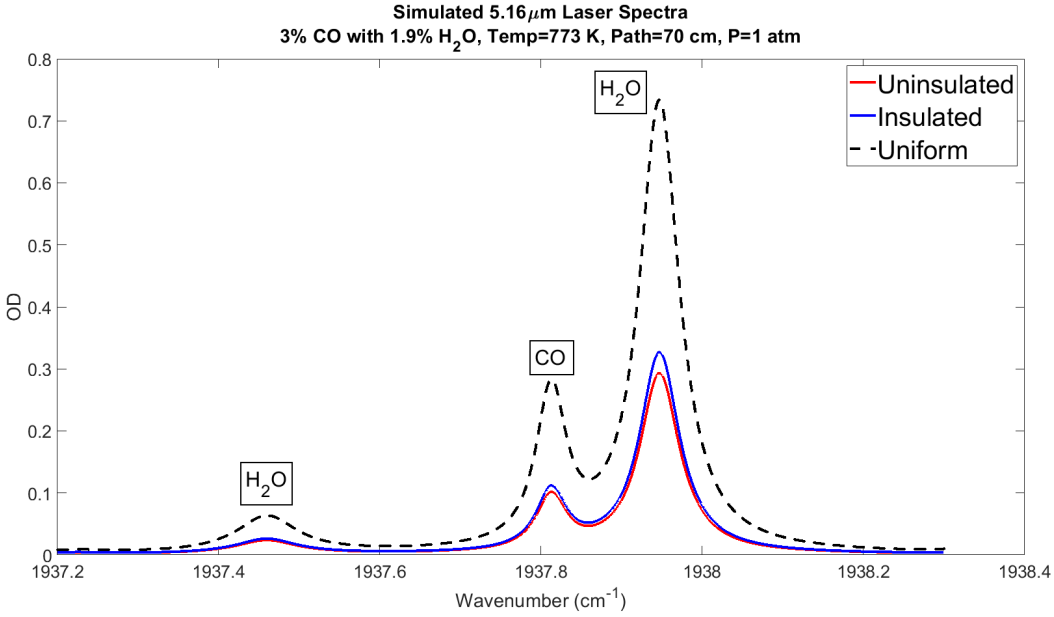

Figure 4.6: WinOSC simulated spectra for 3% CO and 1.9% H_2O at 773 K for a 5.16 μm laser.

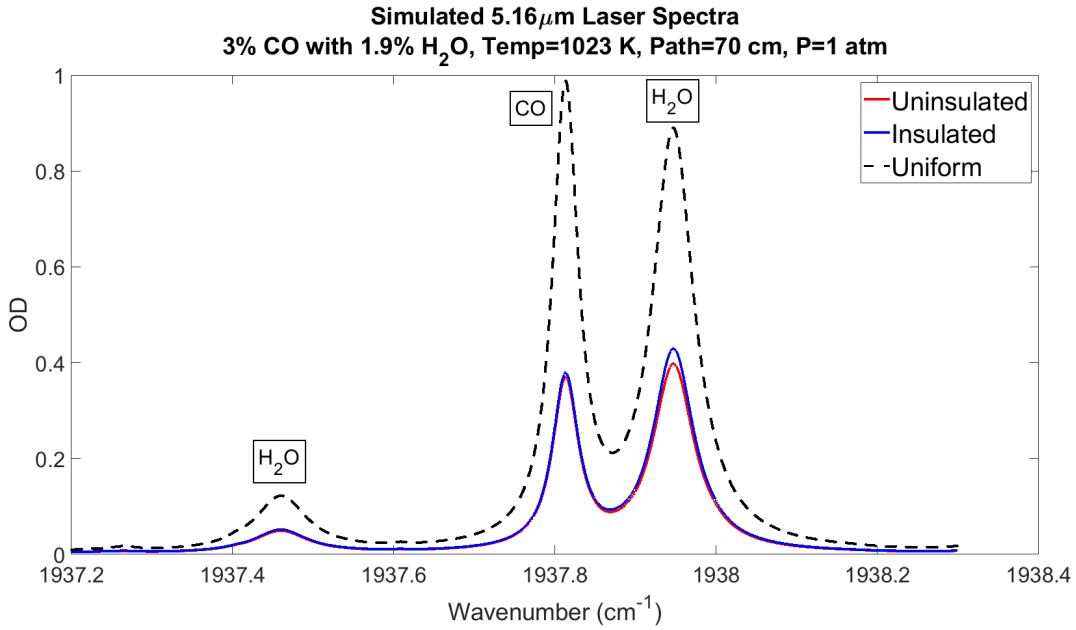

Figure 4.7: WinOSC simulated spectra for 3% CO and 1.9% H_2O at 1023 K for a 5.16 μm laser.

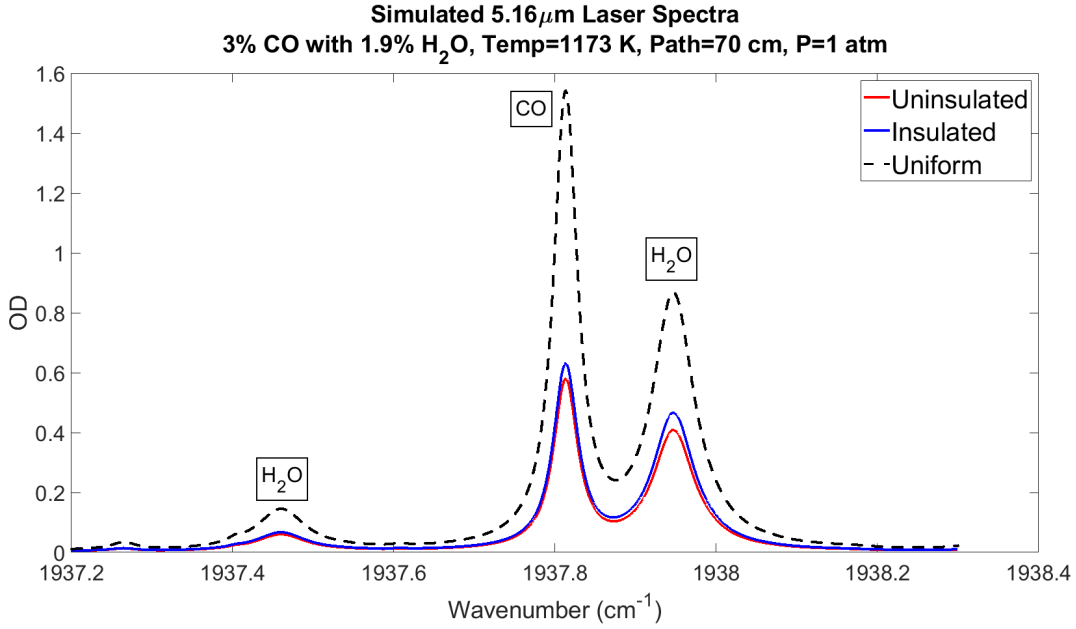

Figure 4.8: WinOSC simulated spectra for 3% CO and 1.9% H_2O at 1173 K for a 5.16 μm laser.

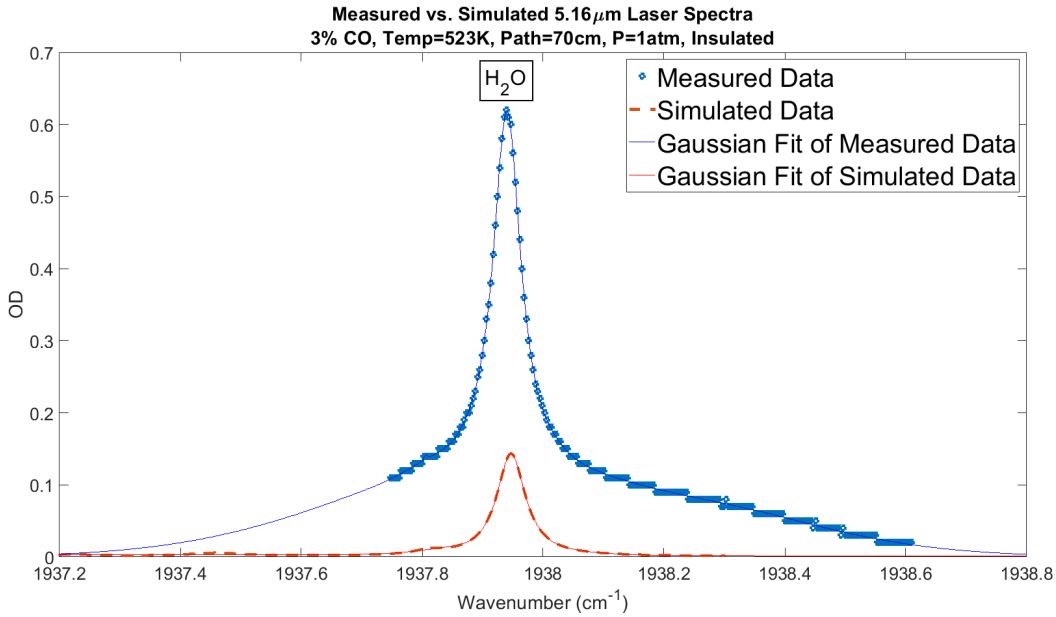

(a) with insulation

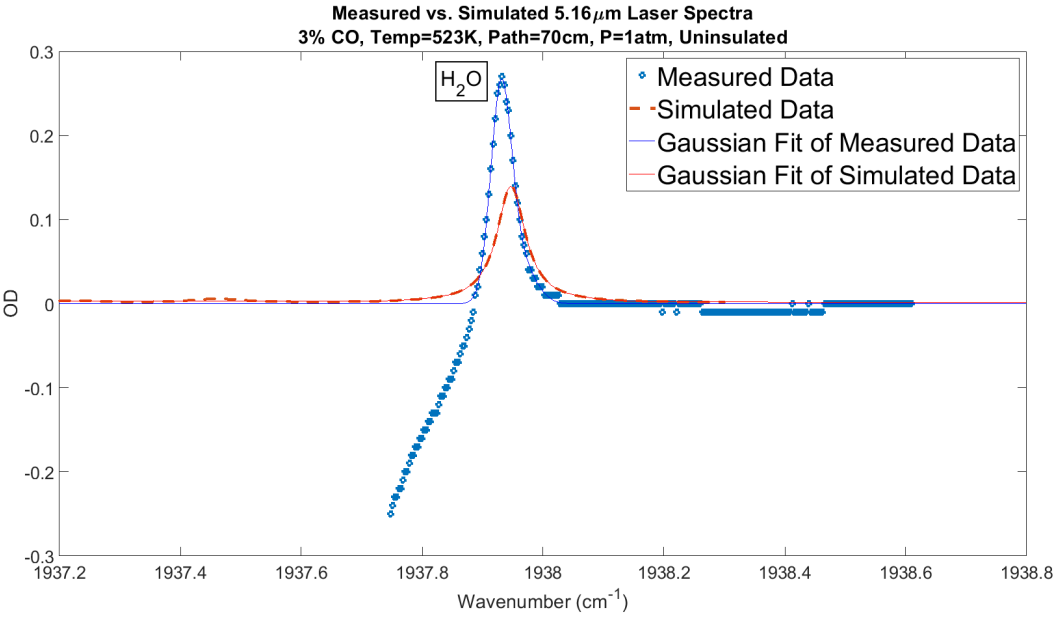

(b) without insulation

Figure 4.9: Measured vs. simulated spectra for 3% CO at 523 K with and without insulation for atmospheric pressure and a path length of 70 cm.

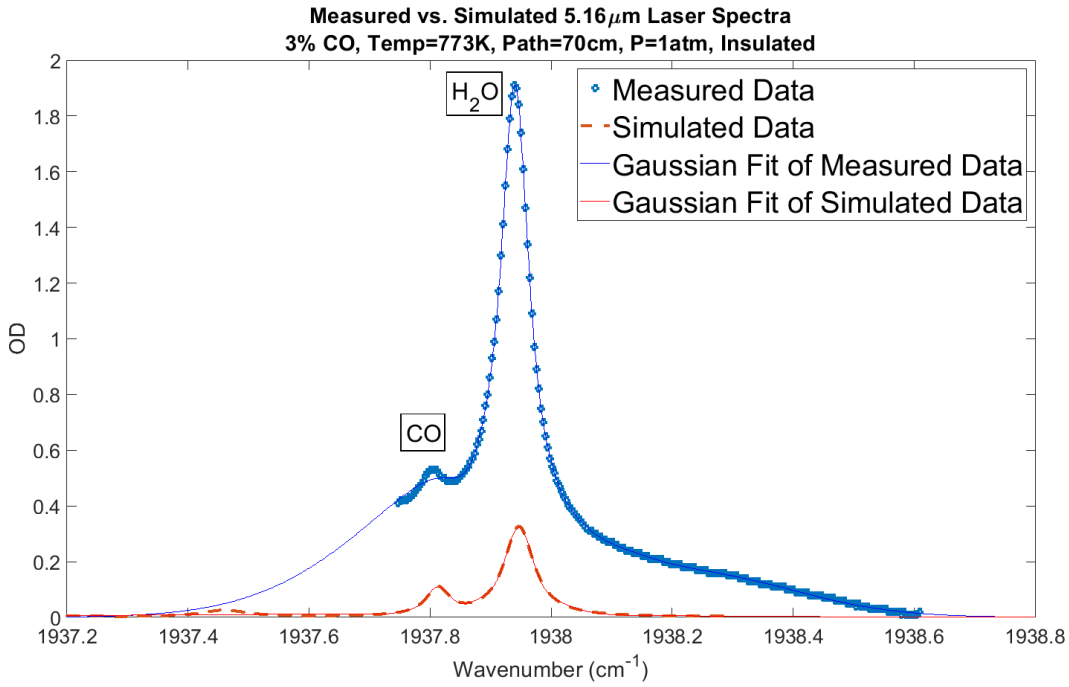

(a) with insulation

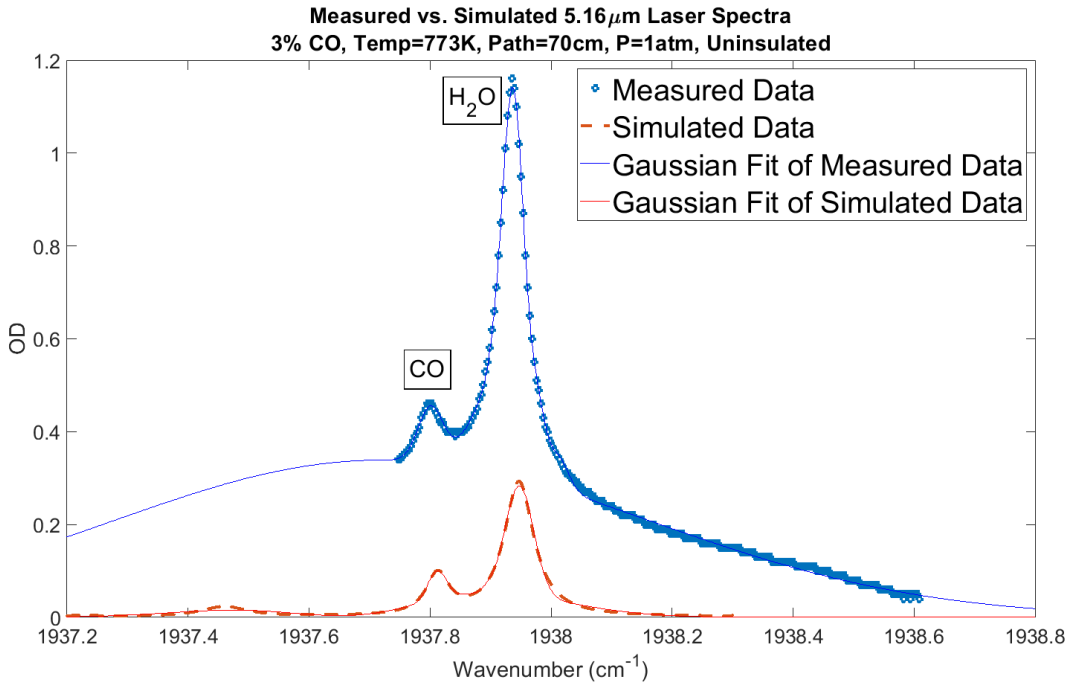

(b) without insulation

Figure 4.10: Measured vs. simulated spectra for 3% CO at 773 K with and without insulation for atmospheric pressure and a path length of 70 cm.

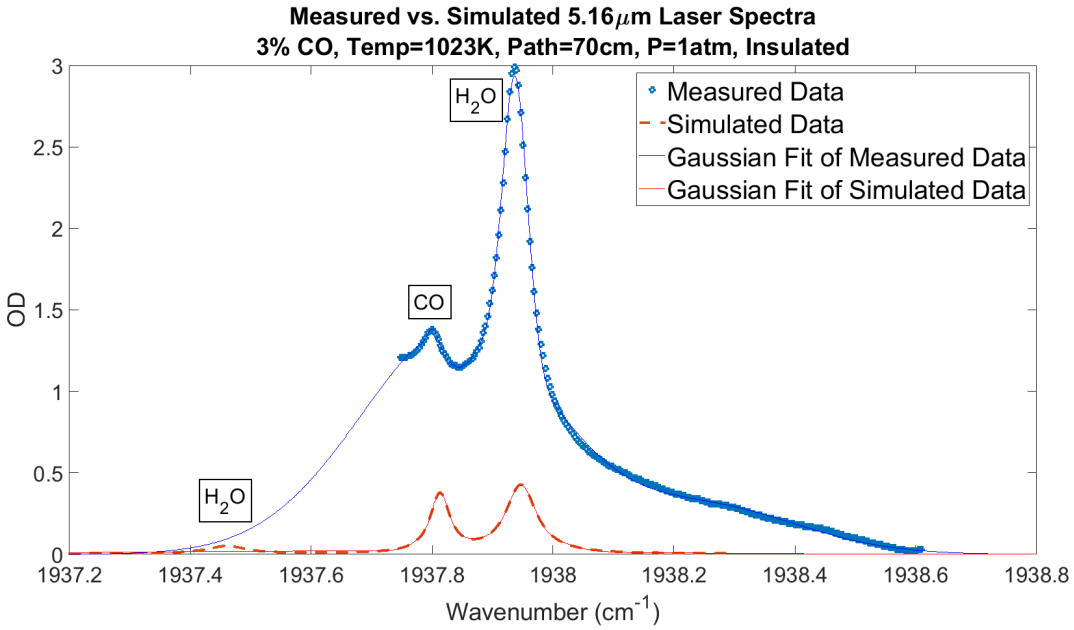

(a) with insulation

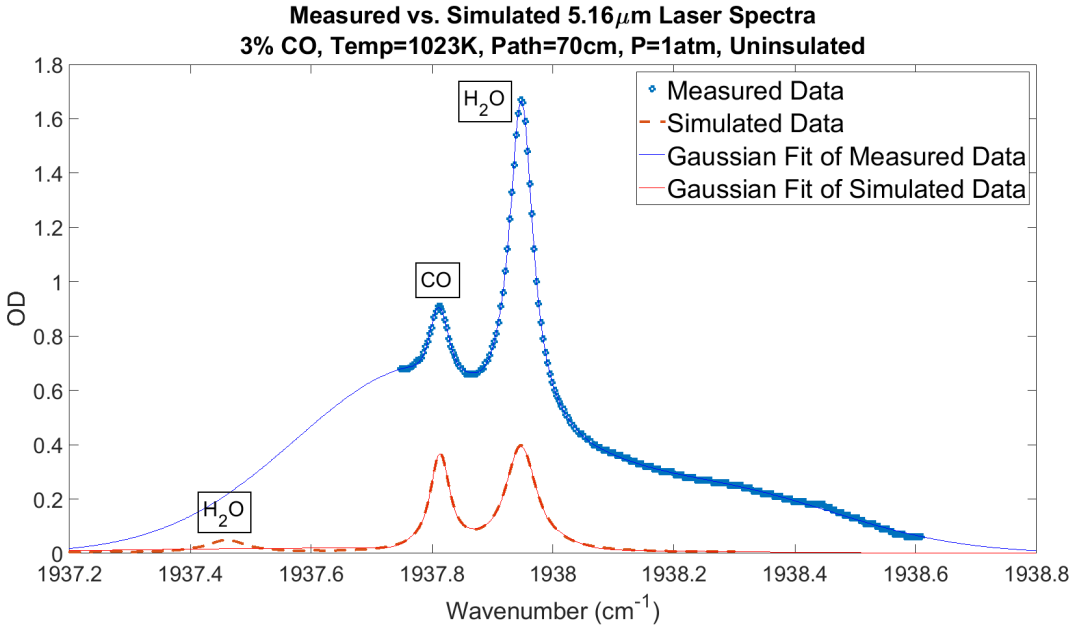

(b) without insulation

Figure 4.11: Measured vs. simulated spectra for 3% CO at 1023 K with and without insulation for atmospheric pressure and a path length of 70 cm.

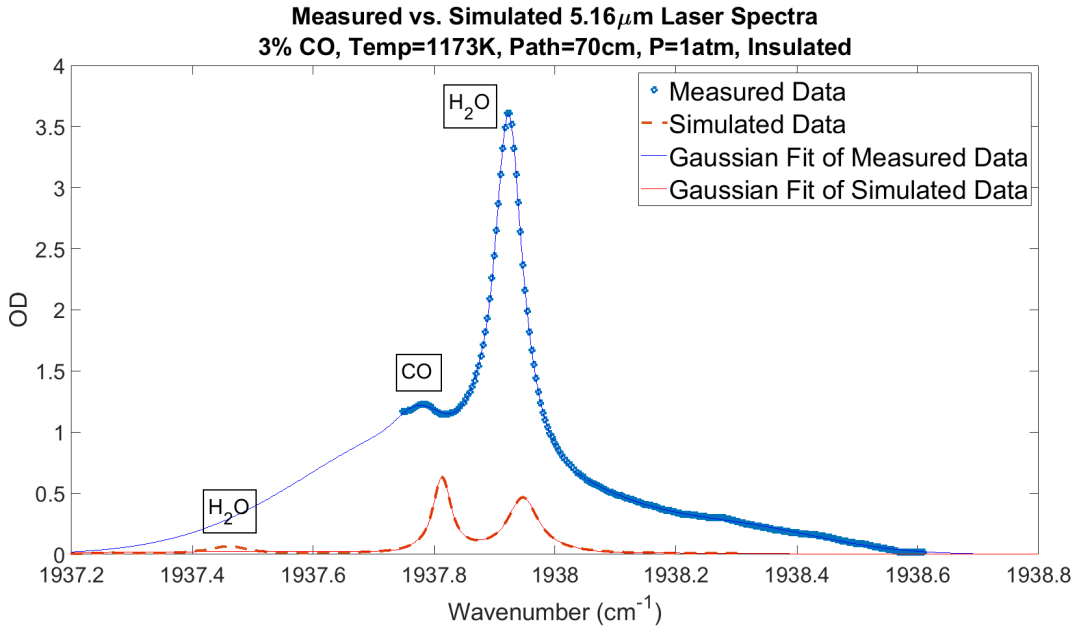

(a) with insulation

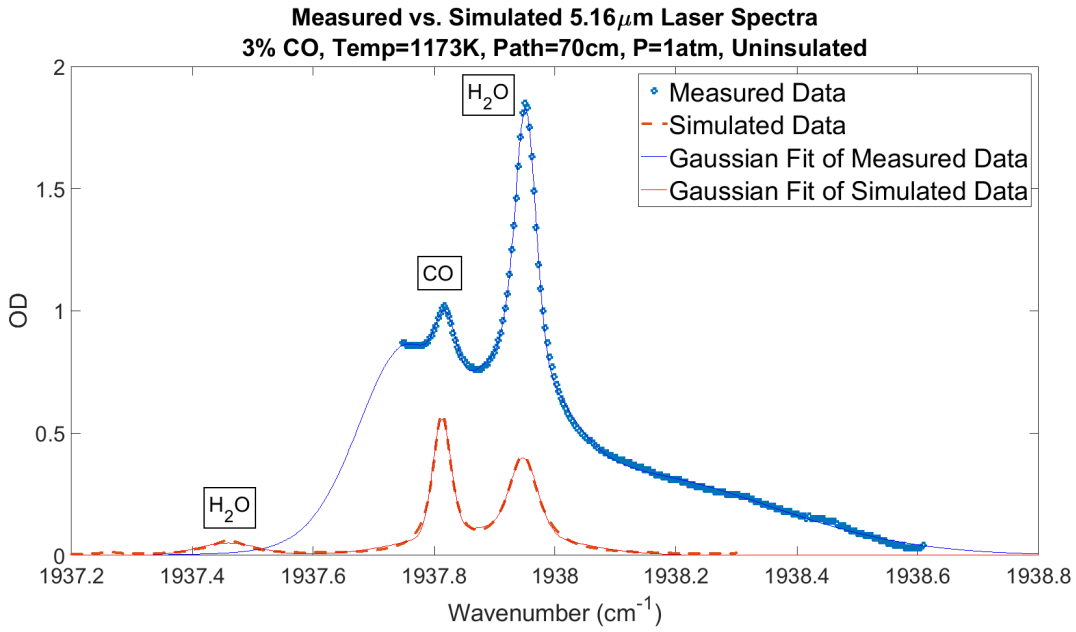

(b) without insulation

Figure 4.12: Measured vs. simulated spectra for 3% CO at 1173 K with and without insulation for atmospheric pressure and a path length of 70 cm.

Table 4.1: Goodness of Fit for Measured CO data (insulated)

Furnace Setting [K]	SSE	R-Square	RMSE	SSE (GOV)	RMSE (GOV)
523	0.001851	0.9995	0.002976	195.495	0.133313
773	0.01417	0.9996	0.008294	1900.08	0.415614
1023	0.11	0.9989	0.02277	7036.75	0.799815
1173	0.01928	0.9999	0.009535	8718.83	0.890293

Table 4.2: Goodness of Fit for Measured CO data (uninsulated)

Furnace Setting [K]	SSE	R-Square	RMSE	SSE (GOV)	RMSE (GOV)
523	0.9009	0.4164	0.06385	7.11183	0.025427
773	0.01109	0.9991	0.007232	1122.71	0.319476
1023	0.007649	0.9997	0.006079	2311.44	0.458401
1173	0.03267	0.9991	0.0125	2512.19	0.477892

Tables 4.3 and 4.4 show a comparison of the experimentally measured results of temperature and species concentrations to known values for insulated and uninsulated conditions of 3% CO. Because waterlines are undetectable at room temperature, the system was unable to measure temperature and species concentration at this setting. The percent difference between measured and known temperatures ranged between 0.70% - 84% for the insulated case and 21% - 91% for the uninsulated case. Both cases show that 523 K has the largest percent difference between known and measured temperatures. This is believed due to there being only one measurable waterline and undetectable CO in this temperature range. All insulated temperature measurents showed a reduction in percent difference compared to their uninsulated counterparts. Without considering 523 K, insulated ends had measured temperatures that were within 0.70% - 8.6% of their known temperatures while uninsulated ends ranged between 21% - 59%. The furnace temperature setting of 773 K contained the lowest temperature difference for both insulated and uninsulated ends.

The premixed gas is believed to have a concentration that is close to 3% CO, and the results of the measured concentrations are inconsistent and contain measurements that are obviously incorrect for any of the temperature settings insulated or uninsulated. For the

Table 4.3: Measured results vs. known vaules of temperature and species concentration with insulation.

Furnace Setting [K]	Known Temp. [K]	Measured Temp. [K]	Temp. %Difference	Known %X CO	Measured %X CO	%X CO %Difference
300	300	No Data	No Data	3.00%	No Data	No Data
523	487.40	1192.29	83.93%	3.00%	6.17 x 10^5%	N/A
773	641.57	646.119	0.70%	3.00%	1.11%	91.97%
1023	824.98	756.83	8.62%	3.00%	378.90%	N/A
1173	957.11	1010.33	5.41%	3.00%	0.47%	145.82%

insulated case, CO species concentrations were measured to be 6.17 x 10^5% and 379% for 523 K and 1023 K, respectively. These are not physical. The large concentration measurement for 523 K could possibly be explained by the single measurable water line and undetectable CO at 523 K producing inaccurate results similar to how it did for temperature measurements since mole fractions is a function of temperature as seen in equation (2.12). 379% CO for 1023 K is not physical as well, but it's uncertain as to why the concentration spiked between 773 K and 1173K, which measured 1.11% and 0.47%, respectively. Examining the uninsulated case, measured species concentrations also produced non physical numbers such 2.2 x 10^6% and -32%, but this time for 773 and 1173 K, respectively. 523 K and 1023 K produced physical measurements of 0.05% and 0.25%, respectively. Upon examining the data for physical results only for both insulated and uninsulated conditions, the data with the lowest percent differences between measured and simulated temperatures also produced species concentrations with the lowest percent differences between their measured and simulated values. For insulated ends, a 0.70% temperature difference for 773 K resulted in a 91.97% difference in species concentration measurements, and a 5.41% temperature difference for 1173 K resulted in a 145.82% difference in species concentration measurements. Likewise, for uninsulated ends, a 36.54% temperature difference for 1023 K resulted in a 169.23% difference in species concentration measurements while a 91.43% temperature difference for 523 K resulted in a 193.44% difference in species concentration measurements. Ironically, insulated and uninsulated ends produced results for temperatures that its counterpart was unable to physically produce, so a comparison between the two temperatures can't be effectively made.

Table 4.4: Measured results vs. known vaules of temperature and species concentration without insulation.

Furnace Setting [K]	Known Temp. [K]	Measured Temp. [K]	Temp. %Difference	Known %X CO	Measured %X CO	%X CO %Difference
300	300	No Data	No Data	3.00%	No Data	No Data
523	476.17	1278.09	91.43%	3.00%	0.05%	193.44%
773	602.7	745.44	21.18%	3.00%	2.2 x 10^6%	N/A
1023	777.77	1125.47	36.54%	3.00%	0.25%	169.23%
1173	884.44	483.76	58.57%	3.00%	-32.01%	N/A

Comparing the overall results, excluding non physical data, insulated ends produced comparatively lower temperature percent differences and thus comparatively lower species concentration percent differences. This correlation agrees with what was simulated in Figure 4.4 where an increase in temperature increases the linestrength. However, the insulated case fits got worse with an increase in temperature with the SSE(GOV) ranging from 195 - 8718 compared to uninsulated ranging from 7.11 - 2512. Such high SSE (GOV) doesn't seem to greatly affect measured temperature values but has more of an effect on the measured species concentrations. For what the system was able to physically measure, results indicate that insulation should produce more accurate results, but with the data so scattered and largely non physical, it is hard to ensure if insulation actually contributed to a more accurate species concentration measurement unless more tests were conducted.

4.3 CO_2 Results

The effects of varying temperatures and species concentrations of CO_2 [3633.055 cm^{-1}] are examined in Figures 4.13, which shows simulation results indicating an inverse relationship between the temperature and optical depth and a direct relationship between species concentration and optical depth. The simulations show that 1% CO_2 yields a measurable range between 0.27 and 1.3 for the optical depth of a uniform temperature distribution for the highest and lowest temperature settings, respectively. Increasing the concentration could

potentially risk too large OD at lower temperature settings, so 1% CO was determined to be the appropriate amount to be tested.

Once the desired species concentration was determined, spectral simulations were created to predict the effect that insulation would have on the absorption spectrum (see Figure 4.14 - 4.17). Applying the insulation lowers the optical depth, which becomes more effective as the temperature increases with a 3.7% to 25% difference in OD from room temperature to 1173 K. It is interesting to note that applying the insulation generates a spectra that is almost identical to a uniform spectrum for temperatures of 1023 K and 1173 K. MATLAB's curve fitting tool determined that SSE and RMSE of the measured to uniform spectra for 1023 K to be 1.53 and 0.0174, respectively. Although insulated and uniform spectra are much more in agreement, a direct comparison cannot be made. For example, the uniform spectra in Figure 4.16 indicates that the path-averaged temperature is 1023 K when in reality it is not the case due to the temperature nonuniformity.

Figures 4.18 - 4.21 plot the measured spectra compared to simulated spectra. The measured optical depth is greater than simulated optical depth for all temperature settings for both insulated and uninsulated. Similar to the measured vs. simulated spectra plots for CO, such an increase in OD was due to the temperature nonuniformity. A Gaussian fit for the measured data points indicate a good fit based on Tables 4.5 and 4.6 where SSE is low and R-Square values are 0.99 for both insulated and uninsulated conditions. Based on the SSE(GOV) in Tables 4.5 and 4.6, measured spectra produce a comparitively better fit to simulated spectra for uninsulated cases with SSE (GOV) values ranging between 9.12 - 58.88 compared to the insulated case with SSE (GOV) values that ranged between 9.64 - 278.94.

Tables 4.7 and 4.8 compare the experimentally measured results of temperature and species concentrations to known values for insulated and uninsulated conditions of 1% CO_2. Similar to the CO results, room temperature was unable to produce measurable temperature or species concentration due to lack of detectable water lines. Recall that there are no measurable water lines in the 2.74 μm region. Water lines are still measured from the 5.16 μm region in order to determine temperature. For all temperature settings, both insulated and uninsulated, the system was able to produce more consistent species concentration measurements with physical results. Unlike CO, CO_2 was able to produce physical results

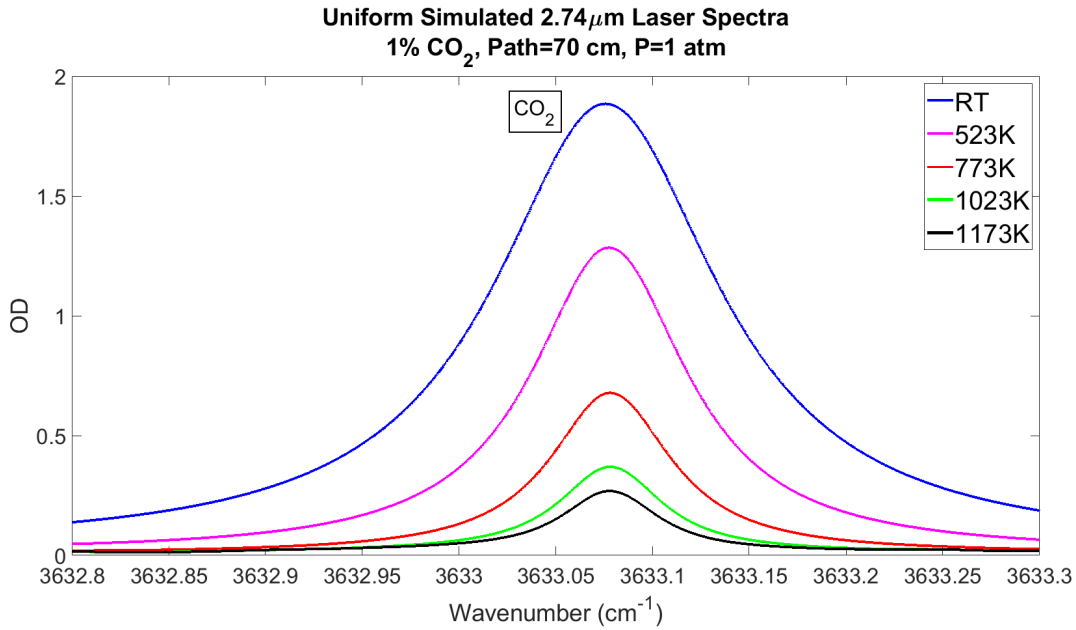

(a) Simulated spectra of 1% CO_2 for room temperature - RT (27 K), 523 K, 773 K, 1023 K, and 1173 K with a path of 70 cm. and pressure of 1 atm.

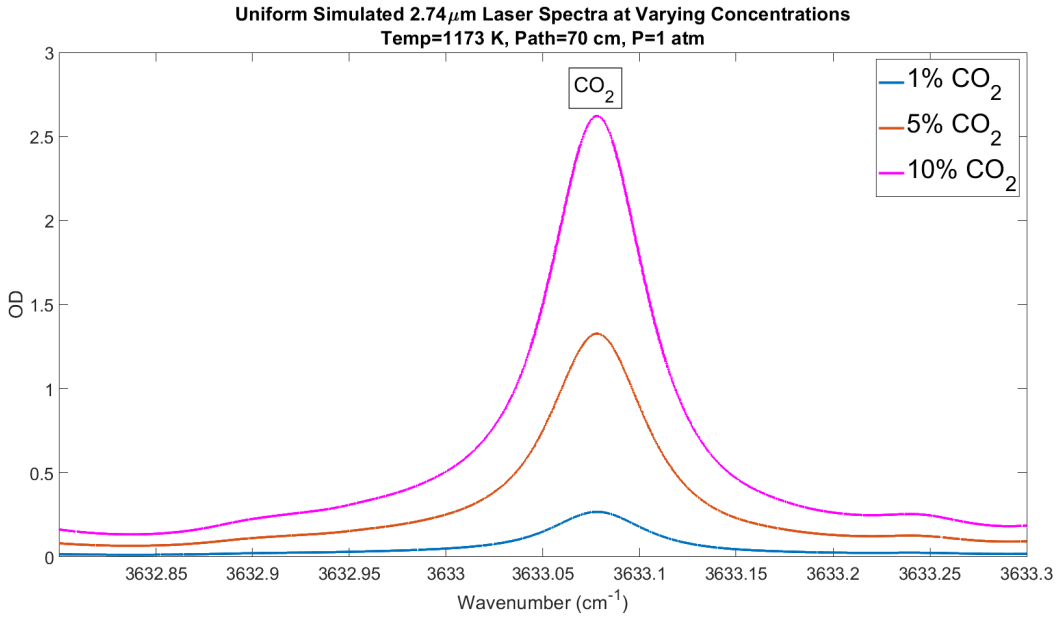

(b) Simulated spectra of 1%, 5%, and 10% CO_2 at 1173 K with a path of 70 cm. and pressure of 1 atm.

Figure 4.13: Simulated spectra used to examine the behavior of CO for different temperatures and species concentrations.

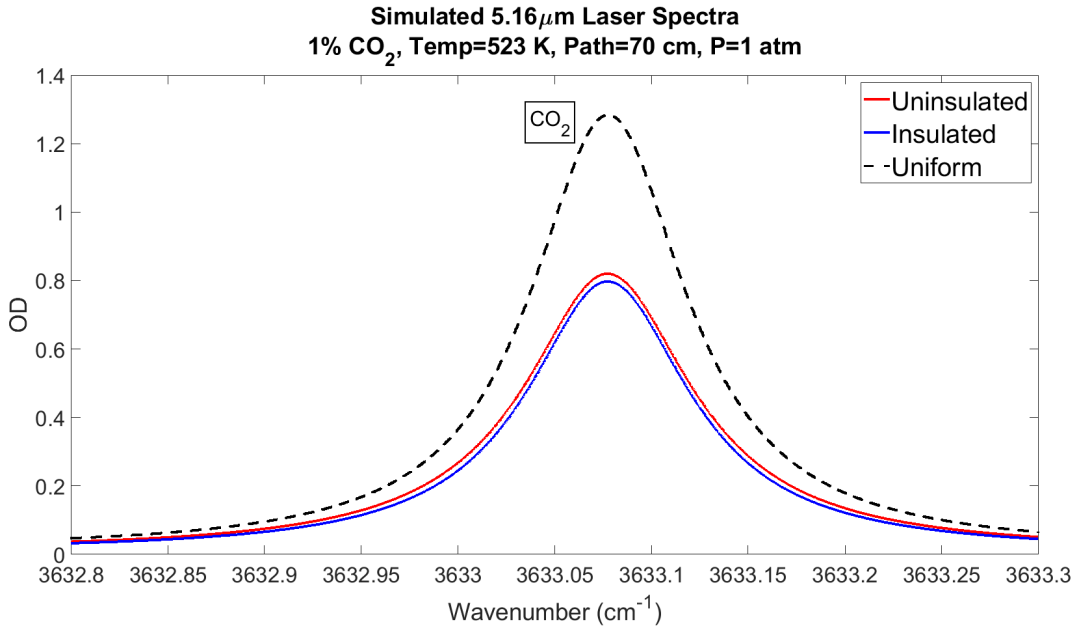

Figure 4.14: WinOSC simulated spectra for 1% CO_2 at 523 K for a 2.74 μm laser.

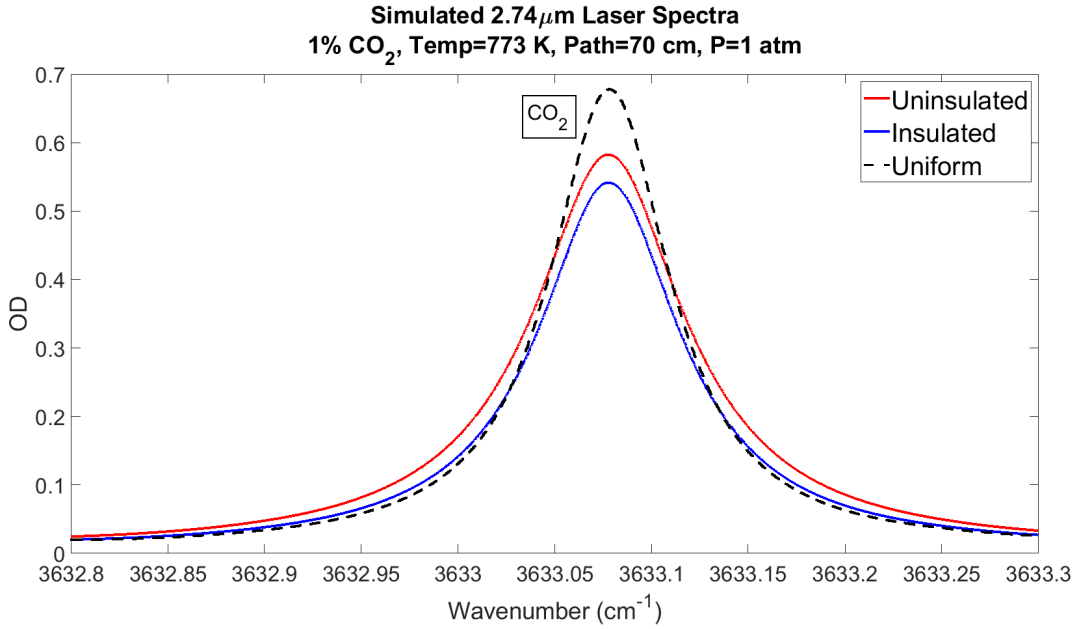

Figure 4.15: WinOSC simulated spectra for 1% CO_2 at 773 K for a 2.74 μm laser.

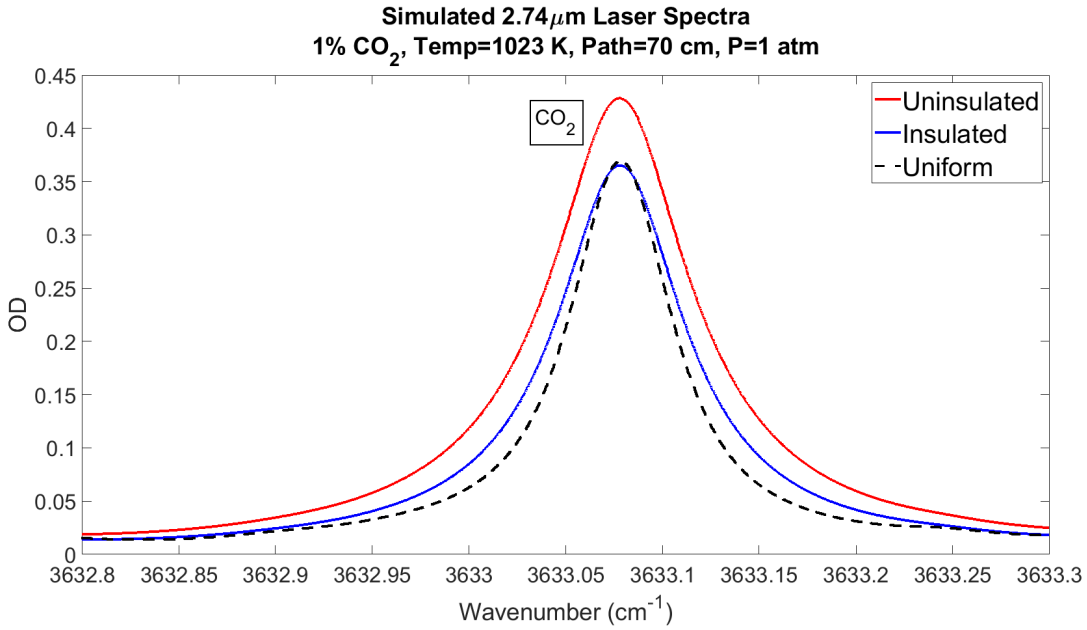

Figure 4.16: WinOSC simulated spectra for 1% CO_2 at 1023 K for a 2.74 μm laser.

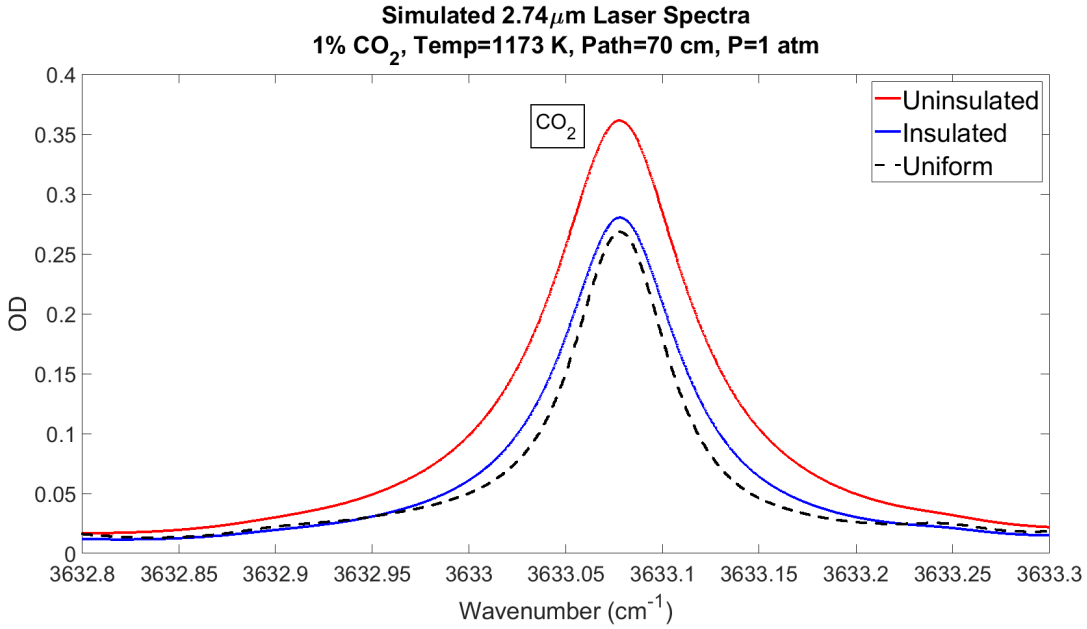

Figure 4.17: WinOSC simulated spectra for 1% CO_2 at 1173 K for a 2.74 μm laser.

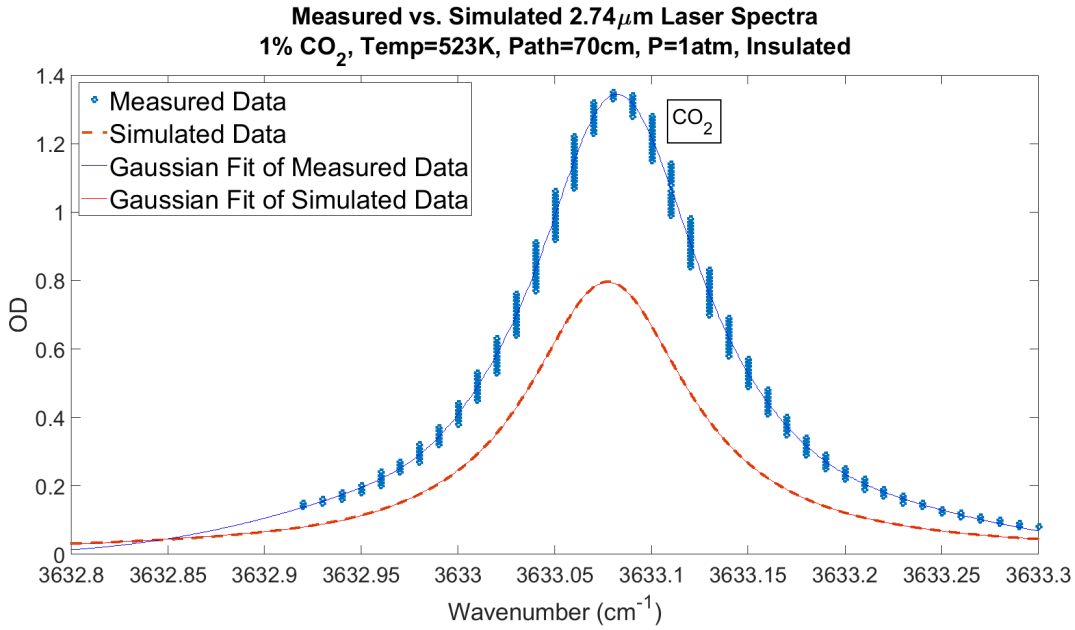

(a) with insulation

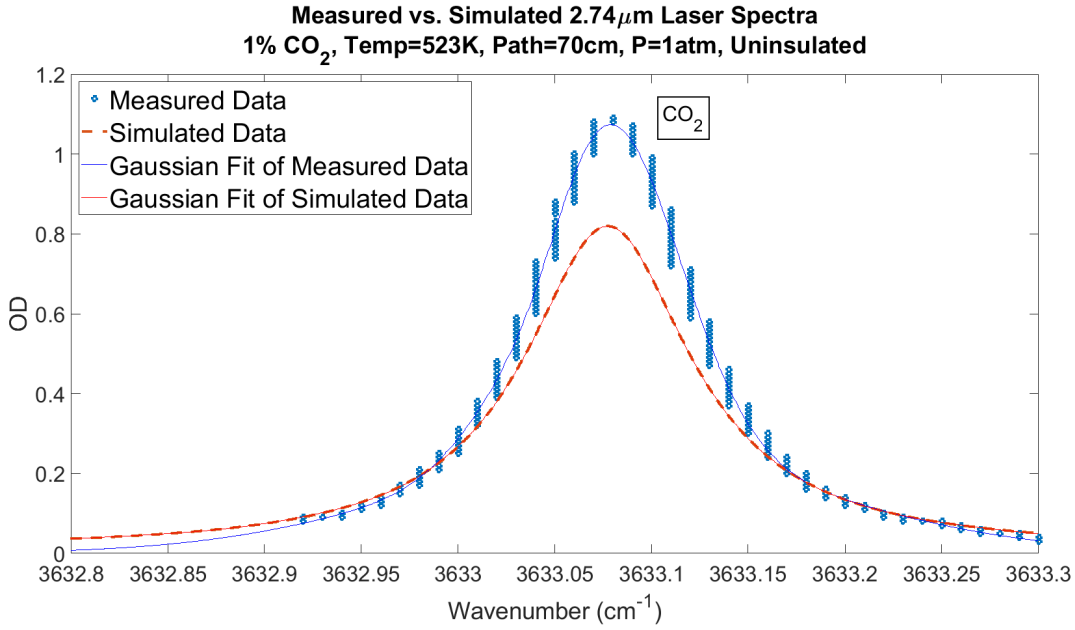

(b) without insulation

Figure 4.18: Measured vs. simulated spectra for 1% CO_2 at 523 K with and without insulation for atmospheric pressure and a path length of 70 cm.

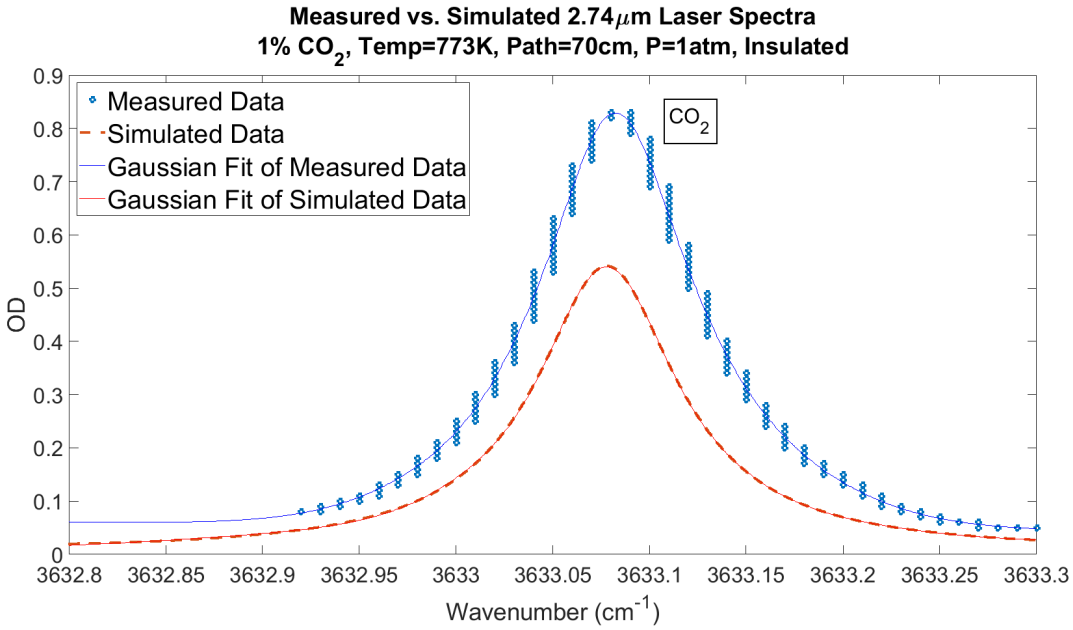

(a) with insulation

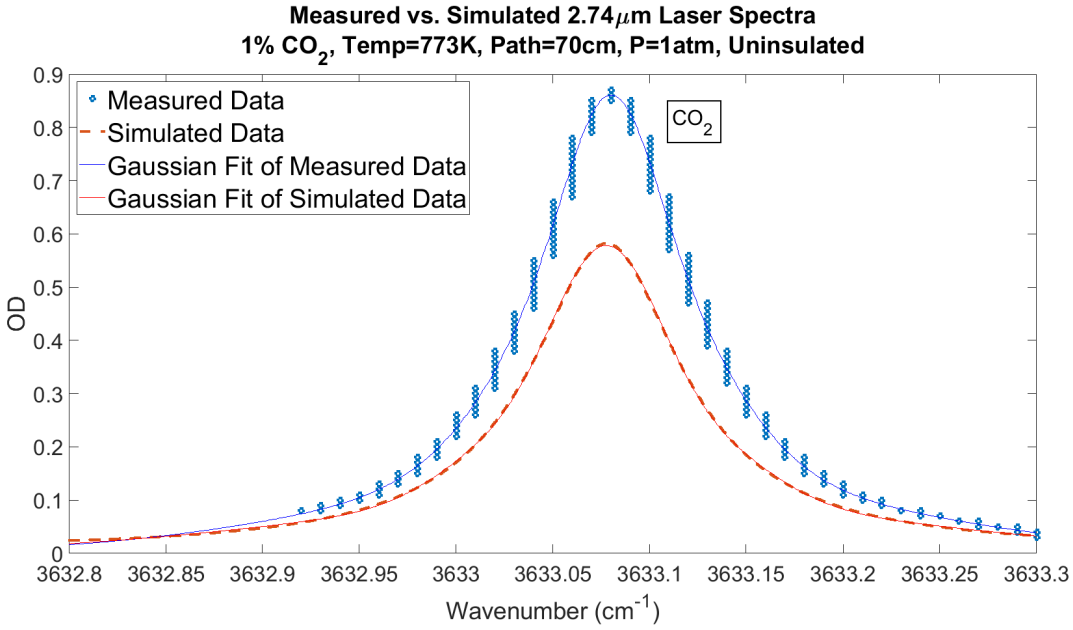

(b) without insulation

Figure 4.19: Measured vs. simulated spectra for 1% CO_2 at 773 K with and without insulation for atmospheric pressure and a path length of 70 cm.

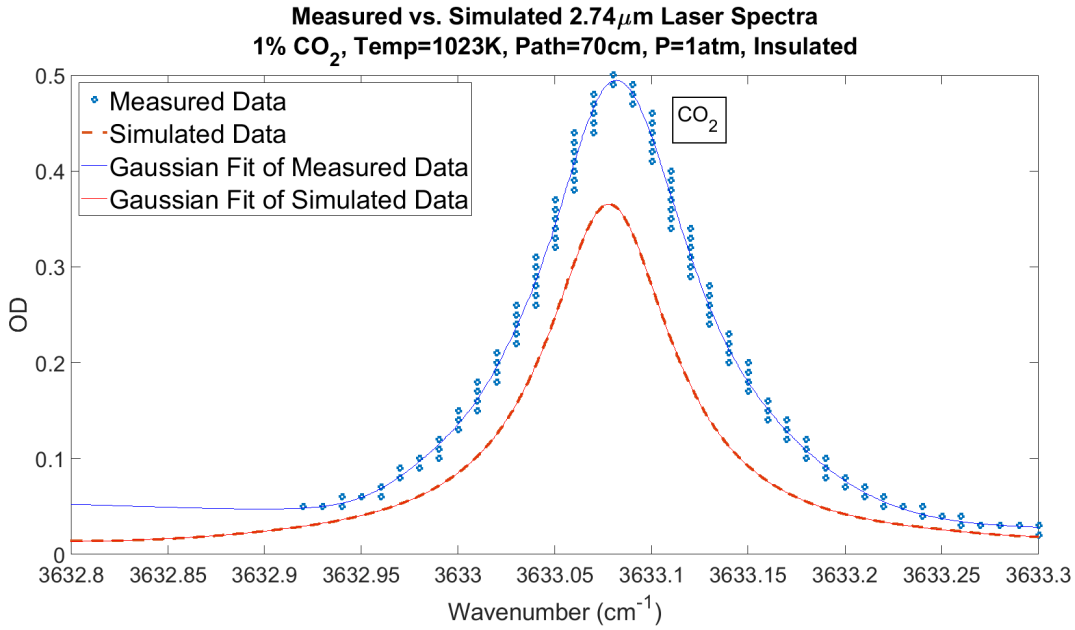

(a) with insulation

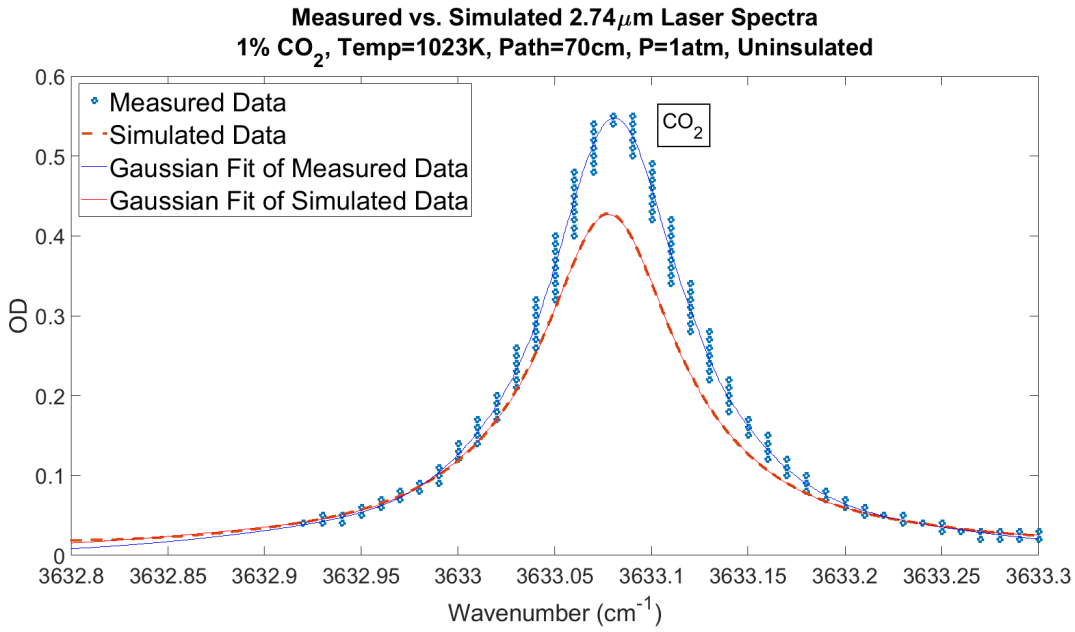

(b) without insulation

Figure 4.20: Measured vs. simulated spectra for 1% CO_2 at 1023 K with and without insulation for atmospheric pressure and a path length of 70 cm.

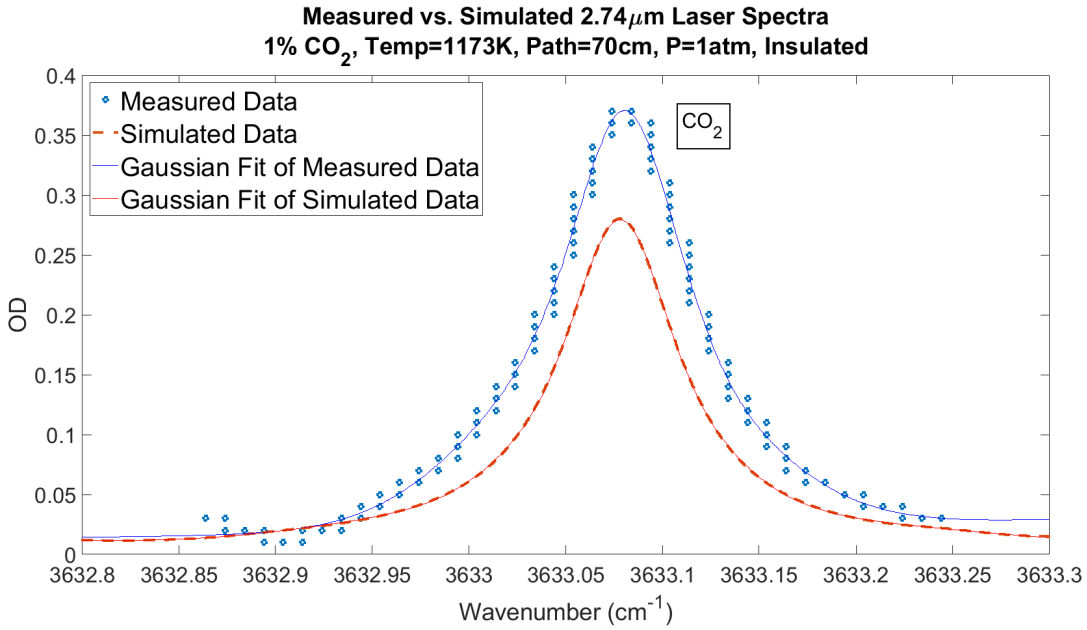

(a) with insulation

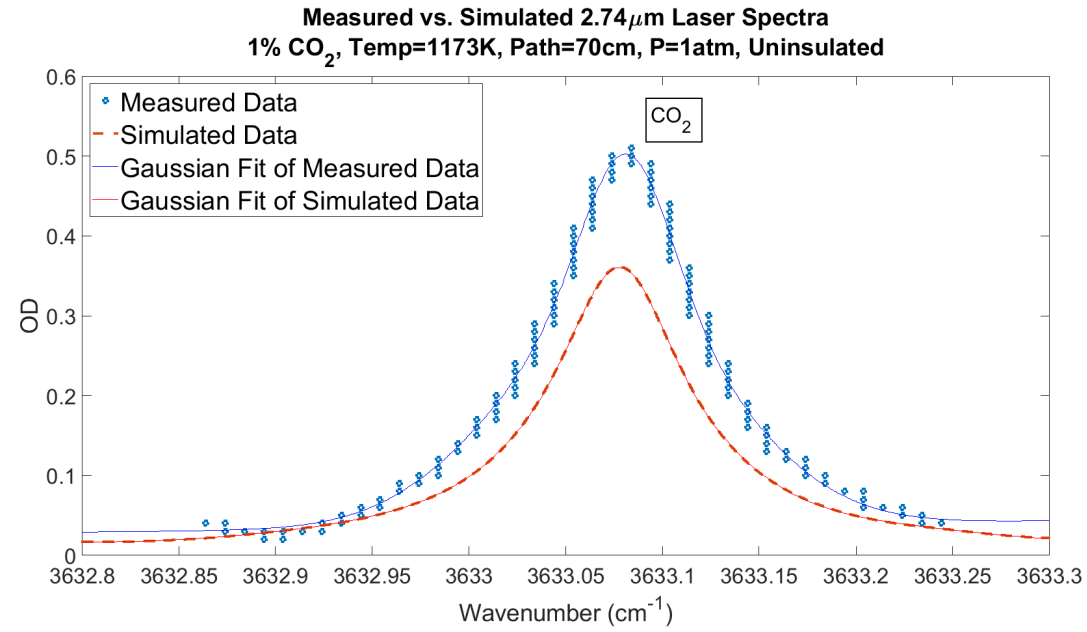

(b) without insulation

Figure 4.21: Measured vs. simulated spectra for 1% CO_2 at 1173 K with and without insulation for atmospheric pressure and a path length of 70 cm.

for 523 K even though there is only one measurable H_2O line. This is most likely due to CO_2, unlike CO, being able to be detected at all furnace temperature settings as shown in Figure 4.13a. Even though 523 K is producing physical results, results indicate this temperature setting produces the second highest temperature percent difference and highest species concentration percent difference for the insulated case. Similarly, 523 K produces the highest temperature and species concentration percent difference for the uninsulated case. The temperature measurement accurarcy for insulated and uninsulated ends ranges between 5% - 45% and 5% - 69%, respectively. Both insulated and uninsulated results indicate that accuracy of temperature and species concentration measurement increases as the furnace temperature increases. Because species concentration is a function of temperature as mentioned in equation (2.12), a decrease in percent difference between measured and simulated temperatures should result in a decrease in percent difference between measured and species concentrations, as shown in Tables 4.7 and 4.8, where there is a general decrease in measured and simulated percent difference of temperature, as the furnace temperature increases, resulting in a percent difference decrease for measured and simulated species concentrations. The trend seems to indicate that applying insulation decreases the overall species concentration measurement accuracy. Without insulation, species concentrations were able to measure within 55% - 155% of the known concentration as opposed to insulated ends measuring 87% - 161%. Uninsulated cases also produced lower percent differences between measured and simulated species concentrations 3 out of 4 times compared to their insulated counterpart. In this case, temperature accuracy for CO_2 is worse with insulation applied as opposed to CO where it increased the accuracy. However, this result is to be expected as shown in Figure 4.13a where the line strength decreases with an increase in temperature.

Table 4.5: Goodness of Fit for Measured CO_2 data (with insulation)

Furnace Setting [K]	SSE	R-Square	RMSE	SSE (GOV)	RMSE (GOV)
523	0.3566	0.9962	0.02469	278.947	0.236198
773	0.1398	0.996	0.01542	83.6275	0.129327
1023	0.05262	0.9958	0.009484	22.8588	0.0676148
1173	0.00483	0.9935	0.008731	9.64246	0.0439146

Table 4.6: Goodness of Fit for Measured data (without insulation)

Furnace Setting [K]	SSE	R-Square	RMSE	SSE (GOV)	RMSE (GOV)
523	0.2842	0.9956	0.02199	44.057	0.0938691
773	0.1661	0.9957	0.01685	58.8853	0.108522
1023	0.08331	0.9946	0.0119	9.12275	0.0427148
1173	0.05887	0.9954	0.01003	18.9036	0.0614876

Table 4.7: Measured results vs. known vaules of temperature and species concentration for CO_2 (with insulation).

Furnace Setting [K]	Known Temp. [K]	Measured Temp. [K]	Temp. %Difference	Known %X CO_2	Measured %X CO_2	%X CO_2 %Difference
300	300	No Data	No Data	1.00%	No Data	No Data
523	487.40	762.73	44.05%	1.00%	9.35%	161.35%
773	641.57	1016.76	45.25%	1.00%	6.30%	145.21%
1023	824.98	1021.81	21.32%	1.00%	3.35%	108.05%
1173	957.11	1008.63	5.24%	1.00%	2.53%	86.69%

Table 4.8: Measured results vs. known vaules of temperature and species concentration (without insulation).

Furnace Setting [K]	Known Temp. [K]	Measured Temp. [K]	Temp. %Difference	Known %X CO_2	Measured %X CO_2	%X CO_2 %Difference
300	300	No Data	No Data	1.00%	No Data	No Data
523	476.17	976.39	68.87%	1.00%	7.80%	154.54%
773	602.7	746.88	21.36%	1.00%	5.99%	142.78%
1023	777.77	821.56	5.47%	1.00%	4.34%	125.09%
1173	884.44	988.65	11.13%	1.00%	0.57%	54.77%

Chapter 5

Conclusions and Recommendations

5.1 Conclusions

A study was performed on UTSI's laser absorption system to determine how accurately the measured spectra could be used to calculate temperature and species concentration of CO and CO_2 from a high-temperature, single-zone absorption cell with a nonuniform temperature distribution. MaxWool^{TM} HPS ceramic fiber blankets were used to insulate the quartz ends of the absorption cell that were exposed to room temperature in order to determine if reducing the temperature gradient at these locations would effect the accuracy of temperature and species concentrations determined from the measured results. A temperature distribution test for furnace settings of 250°C, 500°C, 750°C, and 900°C was first performed to determine the extent at which the insulated blankets were able to contain the heat loss. Results show that the insulation was most effective around the center of the insulated area and was able to effectively increase the temperature for that position by as much as 120% at a furnace setting of 900°C. Simulated spectra were then generated using WinOSC to predict and later compare the results of a 3% CO/N_2 and 1% CO_2/N_2 mixture. Simulations were used to examine the effects that changing temperatures and species concentrations have on the spectra. Then, using the results from the temperature distribution tests, WinOSC was used to model the spectra for the insulated and uninsulated absorption cell by dividing the nonuniform path into uniform layers. Finally, laboratory tests were conducted to determine how well the models predicted the absorption cell test results

and to determine whether or not reducing the temperature gradient had significant effect on the accuracy of the results by comparing measured spectra to simulated spectra.

The results indicate that insulation produced lower percent differences between measured and simulated temperatures, thus resulting in lower percent differences between measured and simulated species concentrations for CO. CO_2, on the other hand, demonstrated an inconsistency in the temperature measurements with insulation improving measurement accuracy half of the time. However, CO_2 showed much more reasonable species concentration measurements, as opposed to CO, and showed that applying the insulation actually decreases the overall accuracy of species concentration measurements. Examining the overall effectiveness of the insulation, it is hard to say whether a reduced temperature gradient results in overall better accuracy. On one hand, it showed improvements in temperature measurement accuracy of CO but half effective for CO_2. Species concentrations measurements produced non physical results for CO half of the time, and CO_2 showed worse results because of insulation. For the most part, the simulated spectra do agree with the results for what the system was able to physically measure. Temperature simulation for CO indicated an increase in linestrength with an increase in temperature, which resulted in lower percent differences between measured and simulated temperatures and thus lower percent differences for measured and simulated species concentrations. CO_2, on the other hand, experiences the opposite effect whereas an increase in temperature results in a decrease in line strength. This is most likely why the overall results of CO_2 seem to indicate that applying the insulation resulted in an overall increase in percentage difference of measured and simulated temperatures thus resulting in an overall increase in percentage difference measured and simulated species concentrations. More testing is probably required to determine the consistency of results. While precautions were taken to prevent contaminating the results, such as vacuum purging the gas tank before premixing and nitrogen purging the absorption cell and laser/detector setup, it's probably best to assume that it's impossible to rid of all contaminants. Therefore, some error in the results is to be expected. The post processor also has many issues that adds to the uncertainty of the results. As shown in Section 4, the measured data can give realistic concentrations, impossible concentrations, and sometimes it fails to measure any concentration. Due to the system producing non

physical and often inconsistent measurements, it is probably best to focus on developing a better correction system instead of continuing to work with insulated ends alone.

5.2 Recommendations for Future Work

UTSI plans to upgrade the current single-zone absorption cell to a more reliable three-zone absorption cell for the study of combustion products in the mid-infrared. The current absorption cell suffers from large temperature nonuniformities that skew the measured results, even with the insulation applied, making further work with this current system difficult to produce any meaningful data. However, if work is still to be done with this current absorption cell setup, a few recommendations are made.

Insulation was used to reduce the temperature nonuniformity but was unable to completely remove it. One could apply heat tape coupled with the thermal insulation to the exposed ends, but this would require water cooling the flanges to take into account the temperature limitation of 232°C for the Kalrez o-ring within the flanges. A uniform temperature of roughly 200°C could possibly be achieved; however, testing at higher temperatures to cover many combustion processes is desired. When it comes to upgrades with the current system, one should be wary of the temperature limitations of the cell material and whether or not they become reactive at higher temperatures.

Water concentration is unable to be controlled or monitored with this current setup, so the measurement system produces water concentrations based on bubbler output. While water is not the focus of the research in this thesis, it is still an important species in combustion products that has been studied in previous tests with the current UTSI system. A similar test was performed to compare measured temperature and species concentrations to known values. Experimenting with water required a slightly different setup. A humidifier was designed to create controlled mixtures of N_2-H_2O that flowed through the absorption cell to study the effects of water lines at temperatures of 773 K and 1173 K. A hygrometer was used to measure the humidifier's relative humidity, which was used to determine the mole fraction of H_2O present. Results from this experiment showed measured temperatures and water concentration to be within 3-7% and 2.7% of their known values [2]. One could expand on

this work to determine whether or not applying the insulation would produce more accurate measurements for temperature and species concentration of water. An advantage with this test was that it was able to precisely measure water concentration with the hygrometer, which allowed an accurate comparison to be made between measured and known species concentration beyond that of human precision. Mixture concentrations of CO and CO_2 in this research were calculated with Dalton's Law of Partial Pressures using pressure transducers. Assuming the gases were mixed correctly, there was no other way to confirm the mixture concentration. Also, due to the time it takes to perform these experiments, only three measurements were taken for each temperature of CO and CO_2 with and without insulation. More testing could be done to determine if results are repeatable.

Bibliography

[1] J. Hollas, *Modern Spectroscopy, 4th Edition*. John Wiley & Sons, Ltd, 2004. x, 5, 6

[2] K. M. Sweetland, C. S. Combs, T. M. Moeller, J. D. Schmisseur, R. P. Rhodes, and F. Zhang, "Development of MIR TLAS System with Applications to Reacting Hot Gas Flows," *American Institute of Aeronautics and Astronautics*, 2018. x, 2, 7, 10, 11, 12, 13, 19, 31, 32, 55

[3] T. Johnson, "Analysis of a High-Temperature Spectroscopic Gas Cell Design," Master's thesis, University of Tennessee, Knoxville, 2018. x, 3, 6, 7, 8, 13, 16, 17

[4] M. Smart, "Scramjet Inlets," *NATO*, 2010. 1

[5] X. Liu, J. Jeffries, R. Hanson, K. Hinckley, and M. Woodmansee, "Development of a tunable diode laser sensor for measurements of gas turbine exhaust temperature," *Applied Physics B: Lasers and Optics*, vol. 82, pp. 469–478, 2006. 2, 8, 9, 11, 16

[6] J. A. Nwaboh, O. Werhahn, D. Schiel, P. Ortwein, and V. Ebert, "Laser-spectrometric gas analysis: CO2-TDLAS at 2 μm," *Measurement Science and Technology*, vol. 24, 2013. 2

[7] C. Christiansen, T. Stolberg-Rohr, A. Fateev, and S. Clausen, "High temperature and high pressure gas cell for quantitative spectroscopic measurements," *Journal of Quantitative Spectroscopy & Radiative Transfer*, vol. 169, pp. 96–103, 2016. 3, 13, 15, 16

[8] B. Stuart, *Infrared Spectroscopy: Fundamentals and Applications*. Analytical Techniques in the Sciences, John Wiley & Sons, Ltd, 2004. 4

[9] B. Wheatley, *Applications of Tunable Diode Laser Absorption Spectroscopy to Aerospace Flows*. PhD thesis, The University of Queensland, Australia, 2017. 6, 7, 10

[10] K. M. Busa, *Development of a Tunable Diode Laser Application Tomography and Allication to Scramjet Engines*. PhD thesis, University of Virginia, 2014. 7, 8

[11] M. Bolshov and Y. Kuritsyn Y.A.and Romanovskii, "Tunable diode laser spectroscopy as a technique for combustion diagnostics," *Spectrochimica Acta Part B*, vol. 106, pp. 45–66, 2015. 7, 10, 11

[12] X. Chao, *Development of Laser Absorption Sensors for Combustion Gases*. PhD thesis, Stanford University, 2012. 7, 10

[13] X. Liu, J. Jeffries, and R. Hanson, "Measurement of Nonuniform Temperature Distributions Using Line-of-Sight Absorption Spectroscopy," *American Institute of Aeronautics and Astronautics*, vol. 45, no. 2, pp. 411–419, 2007. 8, 16

[14] R. Spearrin, W. Ren, J. Jeffries, and R. Hanson, "Multi-band infrared CO_2 absorption sensor for sensitive temperature and species measurements in high-temperature gases," *Applied Physics B: Lasers and Optics*, 2014. 9

[15] J. Phillips, D. Plemmons, and N. Galyen, "HITRAN/HITEMP Spectral Databases and Uncertainty Propagation by Means of Monte Carlo Simulation with Application to Tunable Diode Laser Absorption Diagnostics," tech. rep., Arnold Engineering Development Center, 2011. 10

[16] L. S. Rothman, I. E. Gordon, Y. Babikov, A. Barbe, D. C. Benner, P. F. Bernath, M. Birk, L. Bizzocchi, V. Boudon, L. R. Brown, *et al.*, "The HITRAN2012 molecular spectroscopic database," *Journal of Quantitative Spectroscopy and Radiative Transfer*, vol. 130, pp. 4–50, 2013. 10

[17] L. Rothman, I. Gordon, R. Barber, H. Dothe, R. Gamache, A. Goldman, V. Perevalov, S. Tashkun, and J. Tennyson, "HITEMP, the high-temperature molecular spectroscopic database," *Journal of Quantitative Spectroscopy & Radiative Transfer*, vol. 111, pp. 2139–2150, 2010. 10

[18] R. Hanson and J. Jeffries, "Diode Laser Sensors for Ground Testing," *American Institute of Aeronautics and Astronautics*, 2006. 11

[19] W. Phillips, J. Welch, and B. Brashear, "A high-temperature infrared absorption gas sample cell," *Review of Scientific Instruments*, vol. 63, 1991. 13

[20] A. Technology, "Technical Information Clear Fused Quartz," 2015. 13

[21] S. Sanders, J. Wang, J. Jeffries, and R. Hanson, "Diode-laser absorption sensor for line-of-sight gas temperature distributions," *Applied Optics*, vol. 40, 2001. 16

[22] Nutec, "Ceramic Fiber Blanket." http://www.nutec.com/ceramic-fiber-blanket. Accessed: 2019-3-19. 18

[23] MathWorks, "Evaluating Goodness of Fit," 2019. 30

Appendices

Appendix A

Temperature Distribution Test Results and WinOSC Layers

Table A.1: Table of a half profile temperature distribution comparing insulated and uninsulated ends for a furnace setting of $250°C$. (*centerline of absorption cell/furnace)

Measured Position [in.]	Insulated Temperature [°C]	Uninsulated Temperature [°C]	Percent Change
12.00*	252.93	252.42	0.2020%
11.50	252.93	252.42	0.2020%
11.00	252.93	252.42	0.2020%
10.50	252.93	252.42	0.2020%
10.00	252.93	252.42	0.2020%
9.50	252.93	252.70	0.0910%
9.00	252.93	252.53	-0.2367%
8.50	253.58	254.43	-0.3341%
8.00	254.19	255.20	-0.3958%
7.50	255.05	256.20	-0.4489%
7.00	255.42	256.25	-0.3239%
6.50	254.44	255.16	-0.2822%
6.00	250.86	252.02	-0.4603%
5.50	245.53	244.40	0.4624%
5.00	236.10	233.04	1.3131%
4.50	224.78	219.70	2.3122%
4.00	211.72	200.81	5.4330%
3.50	197.22	180.65	9.1724%
3.00	182.72	157.73	15.8435%
2.50	165.52	133.91	23.6054%
2.00	149.08	111.19	34.0768%
1.50	132.21	92.87	42.3603%
1.00	120.21	79.95	50.3565%
0.50	105.92	63.39	67.0926%
0.00	91.30	60.25	51.5353%

Table A.2: Layer inputs used to simulate a nonuniform temperature distribution with uninsulated quartz ends for a furnace setting of 250°C [523 K]

Layer Number	Temperature [K]	Pressure [atm]	Path [cm]
1	526.26	1.1	10.41
2	529.38	1.1	1.30
3	526.74	1.1	1.27
4	511.87	1.1	1.32
5	483.41	1.1	1.24
6	442.34	1.1	1.19
7	395.70	1.1	1.30
8	359.56	1.1	1.24
9	334.97	1.1	1.27

Table A.3: Layer inputs used to simulate a nonuniform temperature distribution with insulated quartz ends for a furnace setting of 250°C [523 K].

Layer Number	Temperature [K]	Pressure [atm]	Path [cm]
1	526.29	1.1	10.11
2	528.39	1.1	1.30
3	525.80	1.1	1.27
4	513.97	1.1	1.24
5	491.40	1.1	1.22
6	463.12	1.1	1.30
7	430.45	1.1	1.30
8	399.36	1.1	1.30
9	371.765	1.1	1.30

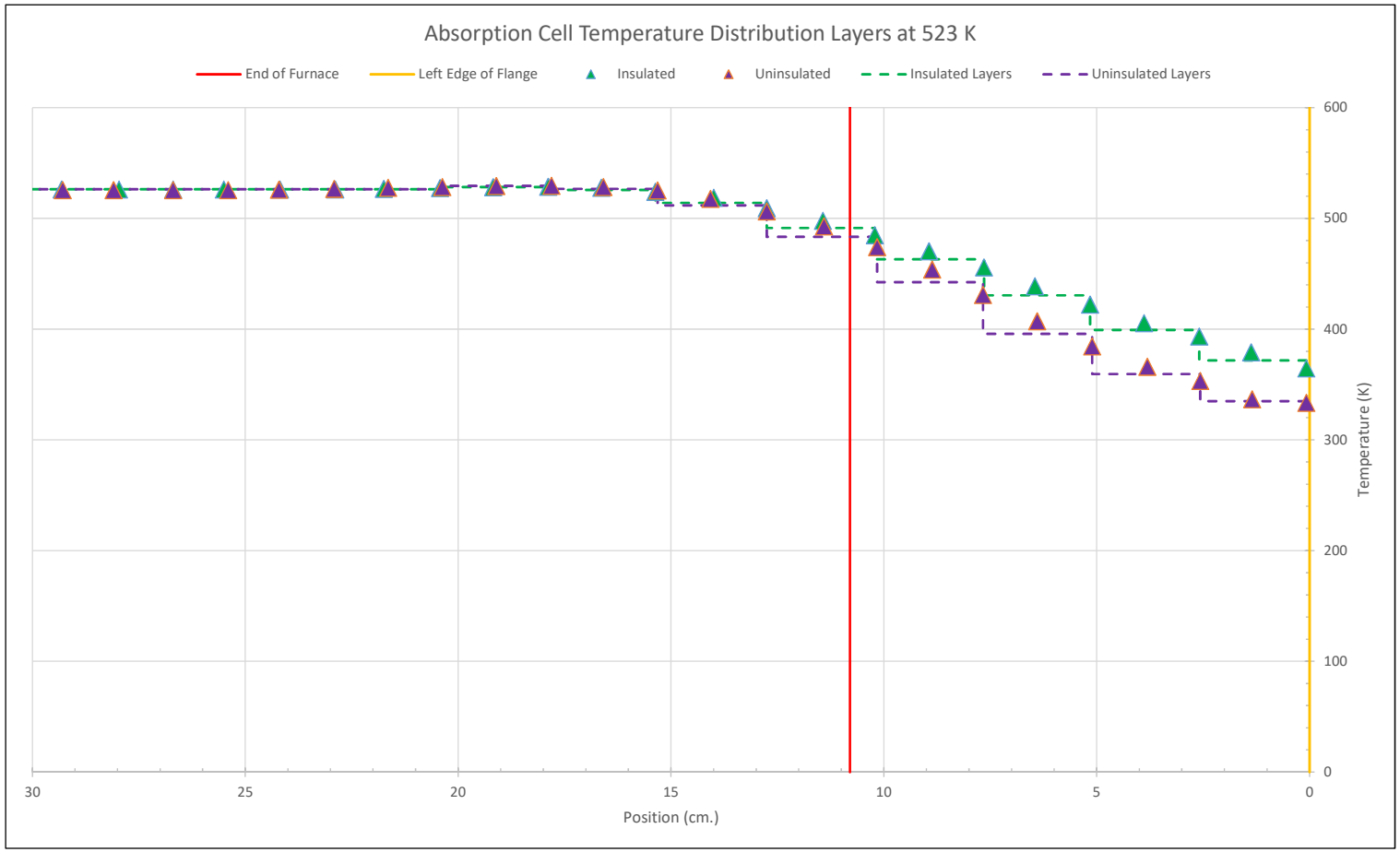

Figure A.1: This plot represents how the layers for a temperature distribution of 523 K were divided for the WinOSC simulations.

Table A.4: Table of a half profile temperature distribution comparing insulated and uninsulated ends for a furnace setting of $500°C$. (*centerline of absorption cell/furnace)

Measured Position [in.]	Insulated Temperature [°C]	Uninsulated Temperature [°C]	Percent Change
12.00*	502.94	502.33	0.1214%
11.50	502.94	502.33	0.1214%
11.00	502.94	502.33	0.1214%
10.50	502.94	502.33	0.1214%
10.00	502.94	502.33	0.1214%
9.50	502.94	502.33	0.1214%
9.00	502.94	502.33	0.1214%
8.50	502.94	502.33	0.1214%
8.00	502.36	499.55	0.5625%
7.50	498.40	491.63	1.3771%
7.00	491.02	474.02	3.3857%
6.50	476.41	447.02	6.5746%
6.00	454.45	406.64	11.7573%
5.50	423.98	358.51	18.2617%
5.00	382.74	311.26	22.9647%
4.50	341.01	255.27	33.5880%
4.00	295.96	199.24	48.5445%
3.50	257.37	158.84	62.0310%
3.00	222.78	131.12	69.9054%
2.50	195.61	110.87	76.4319%
2.00	168.45	95.32	76.7205%
1.50	147.36	81.93	79.8609%
1.00	126.98	72.54	75.0482%
0.50	109.08	65.50	66.5344%
0.00	95.49	59.50	60.4874%

Table A.5: Layer inputs used to simulate a nonuniform temperature distribution with uninsulated quartz ends for a furnace setting of 500°C [773 K].

Layer Number	Temperature [K]	Pressure [atm]	Path [cm]
1	775.23	1.1	10.21
2	756.44	1.1	1.27
3	699.98	1.1	1.02
4	608.04	1.1	1.17
5	500.41	1.1	1.40
6	418.13	1.1	1.27
7	376.25	1.1	1.22
8	350.39	1.1	1.24
9	335.65	1.1	1.22

Table A.6: Layer inputs used to simulate a nonuniform temperature distribution with insulated quartz ends for a furnace setting of 500°C [773 K].

Layer Number	Temperature [K]	Pressure [atm]	Path [cm]
1	775.76	1.1	10.44
2	767.86	1.1	1.27
3	738.58	1.1	1.22
4	676.51	1.1	1.17
5	591.64	1.1	1.22
6	513.23	1.1	1.27
7	455.18	1.1	1.32
8	410.32	1.1	1.24
9	375.44	1.1	1.22

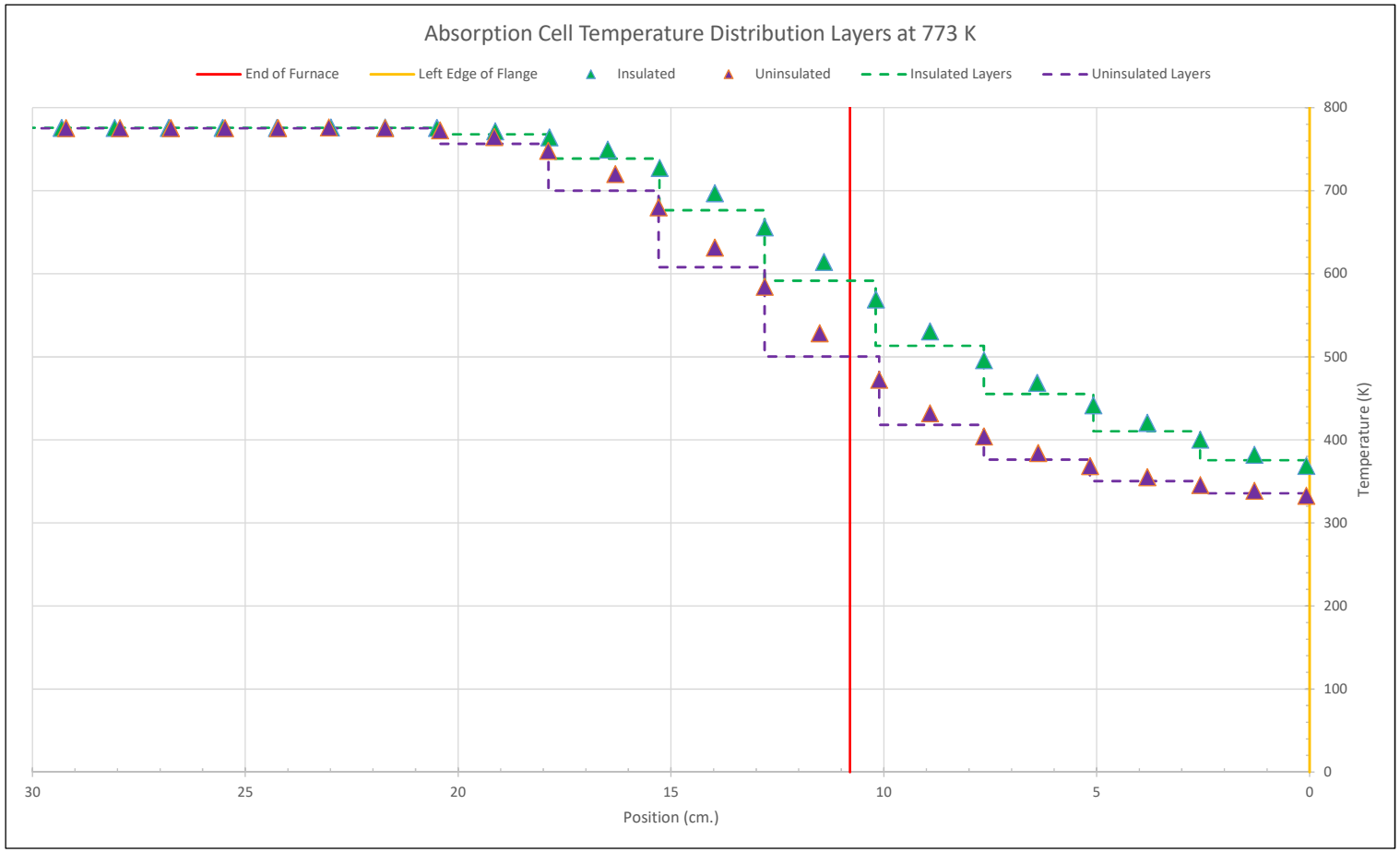

Figure A.2: This plot represents how the layers for a temperature distribution of 773 K were divided for the WinOSC simulations.

Table A.7: Table of a half profile temperature distribution comparing insulated and uninsulated ends for a furnace setting of $750°C$. (*centerline of absorption cell/furnace)

Measured Position [in.]	Insulated Temperature [°C]	Uninsulated Temperature [°C]	Percent Change
12.00*	745.65	745.43	0.0295%
11.50	745.62	745.06	0.0752%
11.00	744.30	744.65	0.0873%
10.50	744.83	744.12	0.0954%
10.00	744.95	743.76	0.1600%
9.50	744.50	743.19	0.1763%
9.00	743.95	742.79	0.1562%
8.50	742.56	742.25	0.0418%
8.00	738.50	740.49	-0.2687%
7.50	729.84	735.12	-0.7183%
7.00	713.62	723.05	-1.3042%
6.50	693.70	698.65	-0.7085%
6.00	662.45	659.35	0.4702%
5.50	623.73	601.55	3.6871%
5.00	576.11	523.57	10.0350%
4.50	521.53	441.02	18.2554%
4.00	468.2	347.92	34.5712%
3.50	414.88	256.75	61.5891%
3.00	361.60	199.8	80.9810%
2.50	318.08	161.38	97.1000%
2.00	273.21	140.69	94.1929%
1.50	233.16	124.15	87.8051%
1.00	196.92	111.05	77.3255%
0.50	168.25	102.77	63.7151%
0.00	144.7	96.89	49.3446%

Table A.8: Layer inputs used to simulate a nonuniform temperature distribution with uninsulated quartz ends for a furnace setting of 750°C [1023 K].

Layer Number	Temperature [K]	Pressure [atm]	Path [cm]
1	1016.68	1.1	10.44
2	1002.24	1.1	1.24
3	952.15	1.1	1.27
4	835.71	1.1	1.35
5	667.62	1.1	1.22
6	501.43	1.1	1.24
7	424.19	1.1	1.24
8	390.75	1.1	1.27
9	372.98	1.1	1.35

Table A.9: Layer inputs used to simulate a nonuniform temperature distribution with insulated quartz ends for a furnace setting of 750°C [1023 K].

Layer Number	Temperature [K]	Pressure [atm]	Path [cm]
1	1017.13	1.1	10.21
2	994.88	1.1	1.35
3	951.23	1.1	1.24
4	873.071	1.1	1.30
5	768.02	1.1	1.22
6	661.39	1.1	1.32
7	568.80	1.1	1.32
8	488.19	1.1	1.22
9	429.63	1.1	1.24

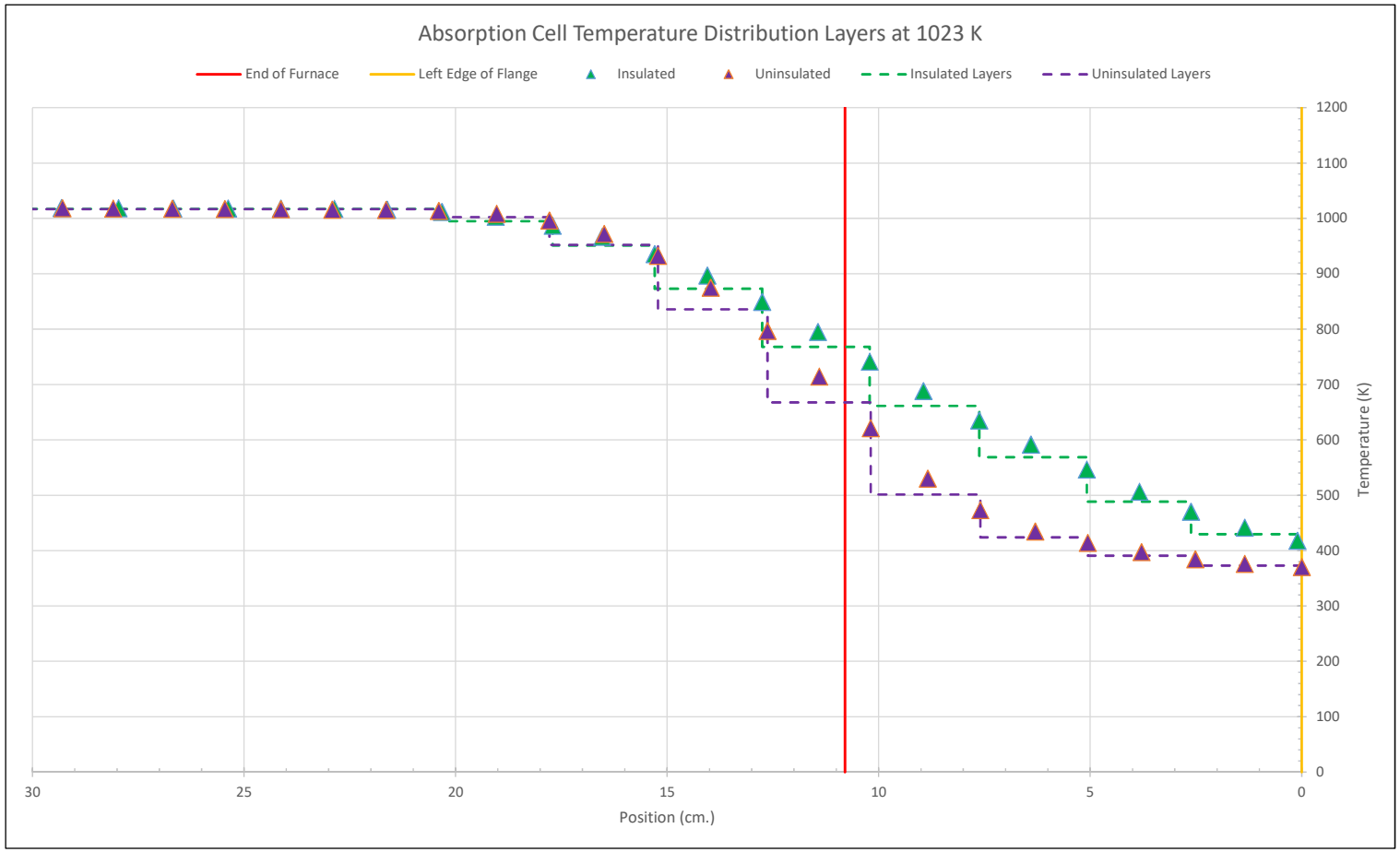

Figure A.3: This plot represents how the layers for a temperature distribution of 773 K were divided for the WinOSC simulations.

Table A.10: Table of a half profile temperature distribution comparing insulated and uninsulated ends for a furnace setting of $900°C$. (*centerline of absorption cell/furnace)

Measured Position [in.]	Insulated Temperature [°C]	Uninsulated Temperature [°C]	Percent Change
12.00*	893.56	892.01	0.1738%
11.50	893.11	891.13	0.2222%
11.00	892.60	890.19	0.2707%
10.50	892.21	889.38	0.3182%
10.00	891.02	887.81	0.3616%
9.50	890.44	886.76	0.4150%
9.00	888.95	885.54	0.3851%
8.50	886.95	883.72	0.3655%
8.00	882.94	880.73	0.2509%
7.50	874.21	874.85	-0.0732%
7.00	860.34	861.59	-0.1451%
6.50	838.62	838.67	-.0060%
6.00	805.11	802.78	0.2902%
5.50	768.29	745.30	3.0847%
5.00	717.13	663.05	8.1562%
4.50	664.64	567.16	17.1874%
4.00	609.66	437.05	39.4943%
3.50	554.52	328.10	69.0094%
3.00	499.13	251.20	98.6982%
2.50	442.12	201.56	119.3491%
2.00	387.79	172.40	124.9362%
1.50	335.45	152.76	119.5928%
1.00	281.75	138.94	102.7854%
0.50	241.96	132.12	83.1365%
0.00	203.43	127.50	91.9059%

Table A.11: Layers used for a furnace setting of 1173 K with uninsulated quartz ends.

Layer Number	Temperature [K]	Pressure [atm]	Path [cm]
1	1160.62	1	10.26
2	1141.37	1	1.32
3	1093.88	1	1.24
4	977.33	1	1.27
5	775.26	1	1.35
6	562.8	1	1.27
7	460.13	1	1.3
8	419	1	1.3
9	402.96	1	1.27

Table A.12: Layers used for a furnace setting of 1173 K with insulated quartz ends.

Layer Number	Temperature [K]	Pressure [atm]	Path [cm]
1	1163.35	1	10.54
2	1140.43	1	1.22
3	1095.02	1	1.37
4	1015.86	1	1.37
5	910.30	1	1.24
6	799.98	1	1.27
7	688.11	1	1.24
8	581.75	1	1.27
9	497.35	1	1.30

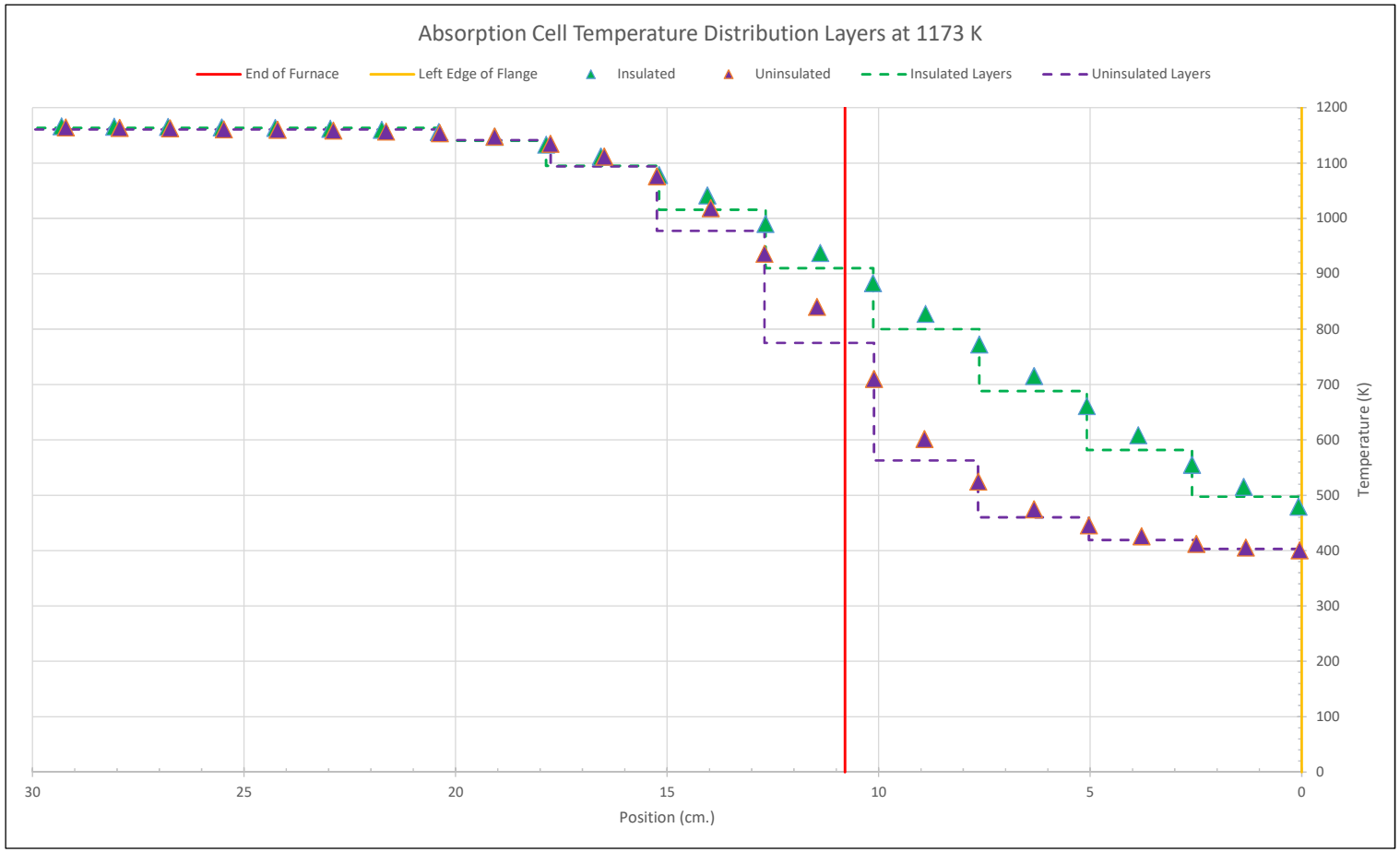

Figure A.4: This plot represents how the layers for a temperature distribution of 1173 K were divided for the WinOSC simulations.

Appendix B

Gas Premixing Procedure

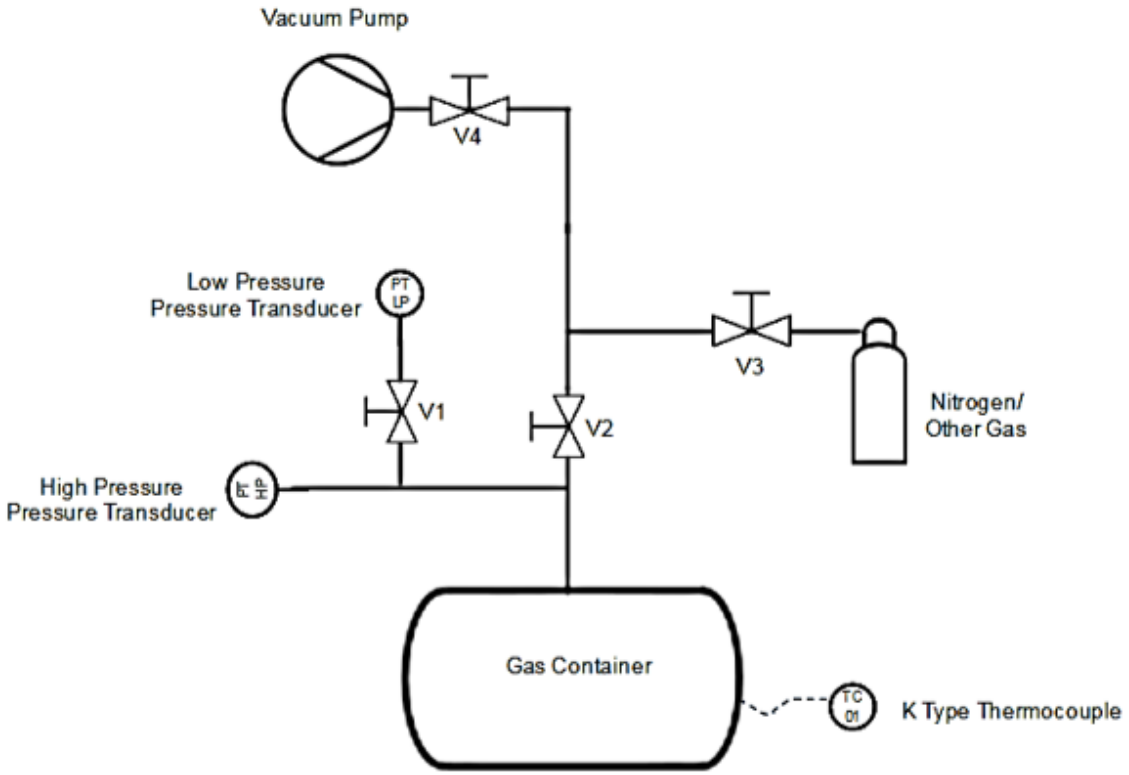

Figure B.1: Schematic of UTSI's gas premixing setup drawn by Katrina Sweetland.

Step 1: Open valves 1, 2, and 4. Close valve 3.

Step 2: Turn on the vacuum pump and draw a vacuum on the gas container for approximately 15 minutes. Use the low pressure transducer to monitor the tank pressure.

Step 3: Close valve 4. Open valve 3 to let nitrogen fill the tank to approximately 15 psia by using the low pressure transducer reading.

Step 4: Once gas container is at approximately 15 psia of nitrogen, close valve 3 and reopen valve 4 so that the vacuum may purge the gas container again.

Step 5: Refill and purge by repeating steps 3 & 4 at least three more times.

Step 6: Close valves 3 and 4. Turn off the vacuum pump. Switch the nitrogen cylinder with either CO or CO_2, depending on which is being tested.

Step 7: Open valve 3. Fill CO or CO_2 to the desired amount using Dalton's Law of Partial Pressures 3.1. Use the low pressure transducer reading to determine how much pressure was added.

Step 8: Close valves 1 and 3. Switch the CO or CO_2 cylinder back to the nitrogen cylinder. (NOTE: it is important that valve 1 is closed so that the transducer does not get damaged in the next step)

Step 9: Open valve 3 and slowly add nitrogen to the required total pressure based on Dalton's Law of Partial Pressure 3.1. Use the high pressure transducer reading to determine that pressure.

Step 10: Close valve 3. Switch the nitrogen cylinder with the line attached to the water bubbler, which has a line that will be attached to the absorption cell. The gas is now premixed and ready for use.

Appendix C

Raw Data Plots

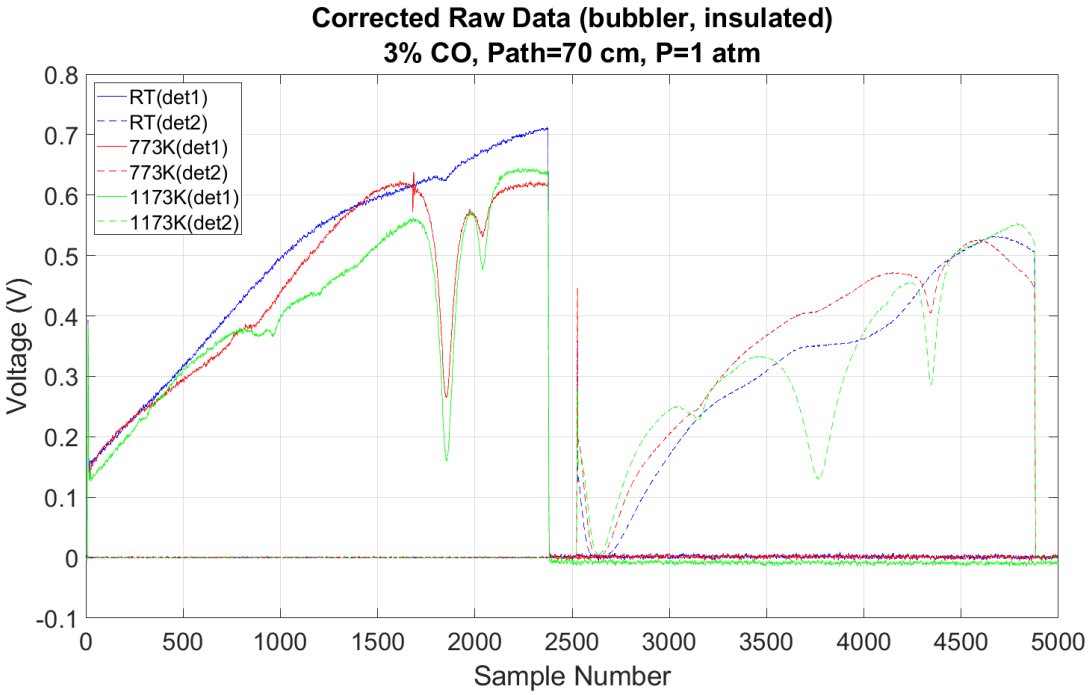

Figure C.1: Corrected DC offset for 3% CO with insulated ends at room temperature, 773K, and 1173K as displayed on the Data Collection LabVIEW. Detector 1 (black line) represents the 5.16 μm laser and detector 2 (red line) represents the 2.74 μm laser.

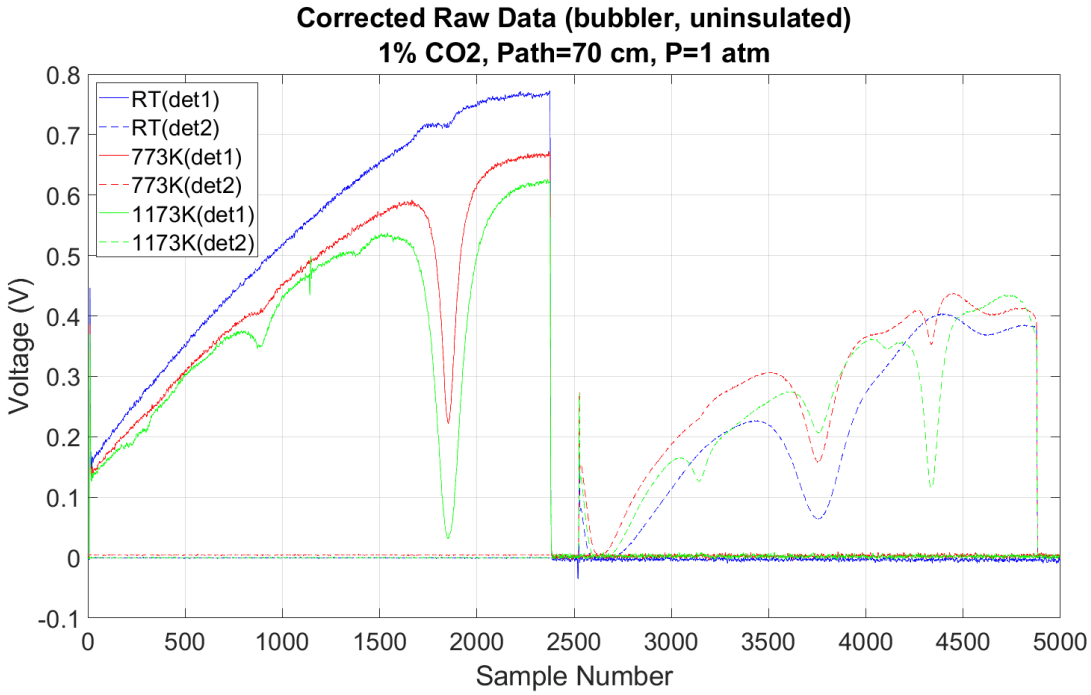

Figure C.2: MATLAB plot for voltage vs. sample number with corrected DC offset for 1% CO_2 for a test cell with uninsulated ends at room temperature (300K), 773K, and 1173K.

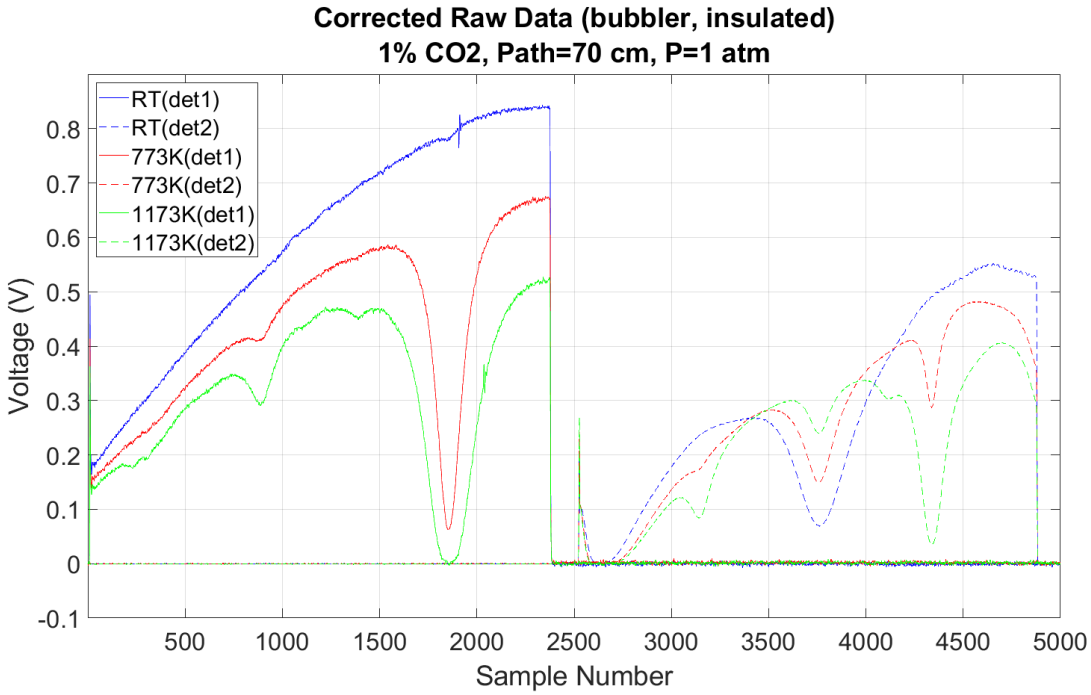

Figure C.3: MATLAB plot for voltage vs. sample number with corrected DC offset of 1% CO_2 for a test cell with insulated ends at room temperature (300K), 773K, and 1173K.

Vita

Waritphon Overacker was born in Nakhon Sawan, Thailand and is the son of Steve and Eht Overacker. He graduated high school in the spring of 2012 and later attended the University of Tennessee at Martin the following fall where he studied engineering with a mechanical concentration. For his senior design project, he was part of the aero design team where he and his team designed and fabricated an RC aircraft that achieved 3rd place in advanced division of the 2016 SAE Aero Design East competition. In the summer of 2016, Waritphon graduated from the University of Tennessee at Martin with a Bachelors in Engineering. Between May and December of 2016, Waritphon interned at Dana Incorporated in Paris, TN as a process engineer where he assisted the other engineers in overseeing the manufacturing of valve covers for commerical and off-highway vehicles. He later began his graduate studies at the University of Tennessee Space Instiute in the spring of 2017 to pursue a Masters of Science in Aerospace Engineering.